UNIVERSITY OF NAPLES FEDERICO II

DOCTORATE IN

MOLECULAR MEDICINE AND MEDICAL BIOTECHNOLOGY

XXXVII CYCLE

Antonella Nostroso

Dissecting the molecular genetics and pathogenesis of dyserythropoiesis in Hereditary Anemias

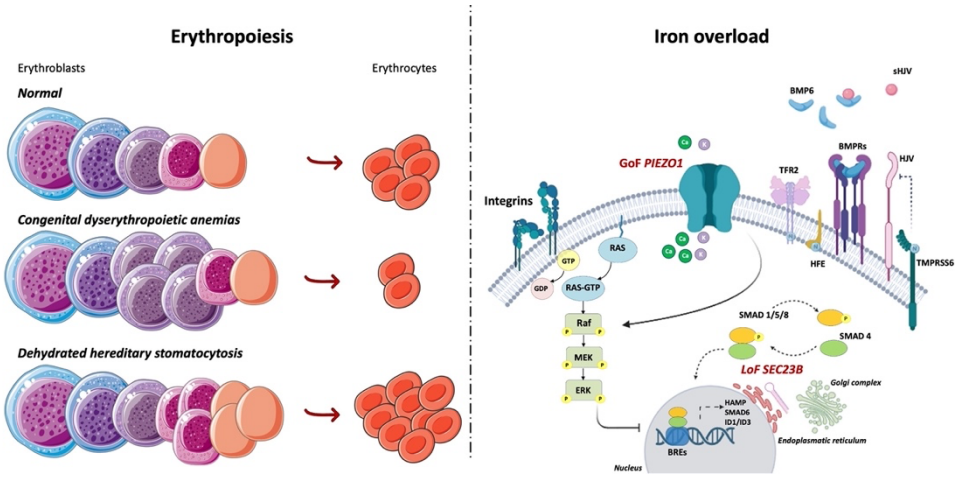

2021-2024

UNIVERSITY OF NAPLES FEDERICO II

DOCTORATE IN

MOLECULAR MEDICINE AND MEDICAL BIOTECHNOLOGY

XXXVII CYCLE

Dissecting the molecular genetics and pathogenesis of dyserythropoiesis in Hereditary Anemias

Tutor

Prof. Roberta Russo

Candidate

Antonella Nostroso

2021-2024

Table of Content

List of abbreviations

ACMG: american college of medical genetics and genomics

AF: alternative allele frequency

ARC: absolute reticulocyte count

BasoE: basophilic erythroblast

BFU-E: erythroid burst-forming unit

BM: bone marrow

BMRI: bone marrow responsiveness index

BMP: bone morphogenetic protein

BP: biological processes

CDA: congenital dyserythropoietic anemia

CDIN1: codanin-1 interacting nuclease 1

CED: C-terminal extracellular domain

CFU-E: erythroid colony-forming unit

COPII: coat protein complex II

CTR: control

DBA: Diamond-Blackfan anemia

DHS: dehydrated hereditary stomatocytosis

DImax: maximum deformability index

EBI: erythroblastic island

EPO: erythropoietin

EpoR: erythropoietin receptor

ER: endoplasmic reticulum

ERFE: erythroferrone

FACS: flow cytometry analysis

FGL1: fibrinogen-like protein 1

FTH: ferritin heavy chain

FTL: ferritin light chain

GAP: GTPase activating protein

GDF11: growth differentiation factor 11

GDF15: growth differentiation factor 15

gDNA: genomic DNA

GoF: gain of function

HA: hereditary anemia

Hb: hemoglobin

HSC: hematopoietic stem cells

HS: hereditary spherocytosis

HSt: hereditary stomatocytosis

HUDEP-2: human umbilical cord blood-derived erythroid progenitors

ICE: inference of CRISPR edits

IE: ineffective erythropoiesis

ID1: inhibitor of DNA binding 1

ID3: inhibitor of DNA binding 3

IFNα: interferon alpha

IL-3: interleukin 3

LDH: high lactate dehydrogenase

LoF: loss of function

MCV: mean cell volume

MCH: mean corpuscular hemoglobin

MCHC: mean corpuscular hemoglobin concentration

MDS: myelodysplastic syndromes

NGS: next-generation sequencing

OD: optical density

OMIM: Online mendelian inheritance in man

OrthoE: orthochromatic erythroblast

PCA: Principal component analysis

PK: pyruvate kinase

PKD: pyruvate kinase deficiency

PolyE: polychromatophilic erythroblast

ProE: proerythroblast

PTM: post-translational modification

RBC: red blood cells

RP: ribosomal protein

SCF: stem cell factor

SDS-PAGE: sodium dodecyl sulfate polyacrylamide gel

shRNA: small hairpin RNA

sTfR: soluble transferrin receptor

SMAD: small mother against decapentaplegic

TEM: transmission electron microscopy

TfR1: transferrin receptor 1

TPD: Treponema pallidum domain

UTR: untranslated region

WB: western blotting

WT: wild type

XLTDA: X-linked thrombocytopenia with or without dyserythropoietic anemia

Abstract

Hereditary anemias (HAs) represent a large group of disorders caused by mutations in genes that regulate hemoglobin production, erythropoiesis, and the structure or metabolism of red blood cells (RBC). In this study, we investigated erythroid maturation defects in three different HA subtypes. Specifically, we focused on congenital dyserythropoietic anemias both type I and II (CDA I-II) and dehydrated hereditary stomatocytosis (DHS). CDA I and II, caused by mutations in *CDAN1*/*CDIN1* or *SEC23B* respectively, are autosomal recessive disorders characterized by defective erythroid differentiation and ineffective erythropoiesis. In contrast, DHS is autosomal dominant anemia caused by gain-of-function mutations in *PIEZO1*, leading to abnormal intracellular cation content and altered cell volume. Despite their distinct pathogenesis, CDAs and DHS share hallmark features, including dyserythropoiesis and iron overload, which represent their main complications. Nowadays, the pathogenic mechanisms underlying these defects are not yet fully elucidated. Thus, the primary aim of this study was to investigate the mechanisms impairing erythroid differentiation using disease cellular models. By using HUDEP-2 erythroid progenitor cells, we demonstrated that loss-of-function mutations in *SEC23B* and *CDIN1* block intermediate-to-late erythroid maturation, while gain-of-function variants in *PIEZO1* enhance erythropoiesis by accelerating the accumulation of mature erythroblasts and promoting enucleation. Transcriptomic analyses revealed stage-specific alterations in shared biological pathways across CDA models, particularly in rRNA processing and ribosome biogenesis. Whereas the DHS model showed an imbalance in glycolytic flux, leading to energy deficits due to reduced ATP production. In parallel, the second aim of this study was to establish a genotype-phenotype correlation in patients with dual inheritance of *SEC23B* (CDA II) and *PIEZO1* (DHS1) mutations. Among a large cohort of 581 HA patients referred for genetic testing, we identified patients carrying pathogenic variants in both genes, a condition termed dual inheritance. Patients with dual inheritance exhibited significantly higher

hemoglobin levels, absolute reticulocyte counts, and bone marrow responsiveness index compared to those with isolated HA subtypes. Additionally, dual patients showed more severe iron overload, with 64% exceeding clinical ferritin thresholds. Accordingly, intermediate erythroferrone levels and markedly reduced hepcidin concentrations in dual-inheritance patients were observed. To further investigate these observations, we developed a hepatic cellular model combining *SEC23B* silencing and *PIEZO1* gain-of-function mutation. Functional assays demonstrated a synergistic effect, including marked *HAMP* downregulation and disruption of the BMP/SMAD pathway compared to cellular models carrying isolated gene defects. This study sheds light on the molecular basis of erythroid dysfunction in hereditary dyserythropoietic anemias and reveals synergistic genetic effects on iron homeostasis, providing insights into improved diagnostics and therapies for hereditary anemias.

1. Background

1.1 Molecular basis of Erythropoiesis and its impairments

Erythropoiesis is a tightly regulated process originating in the bone marrow (BM), characterized by the differentiation of hematopoietic stem cells (HSCs) into mature enucleated red blood cells (RBCs). This complex process spans approximately 14 days in humans and involves 7 to 8 steps across two main phases (Caulier 2022). In the initial phase, HSCs give rise to a group of progenitor cells specifically committed to the erythroid lineage, the burst-forming unit erythroid (BFU-E) cells, which subsequently differentiate into colony-forming unit erythroid (CFU-E) cells. The second phase of erythropoiesis begins with the formation of proerythroblasts (ProE), the earliest morphologically recognizable erythroid precursors. It progresses through distinct stages: basophilic (BasoE), polychromatophilic (PolyE), and orthochromatic (OrthoE) erythroblasts. During this process, the precursor cells exhibit a gradual decrease in both cell and nuclear size, alongside a significant increase in intracellular hemoglobin (Hb) content (Granick 1964). Ultimately, the nucleus condenses and is expelled, leading to the formation of reticulocytes, which are then released into the bloodstream to complete their maturation into fully functional RBCs (Figure 1.1). Reticulocyte maturation is a complex process that results in approximately 20% loss of plasma membrane surface area, reduced cell volume, increased association of the cytoskeleton to the outer plasma membrane, and the loss of all residual cytoplasmic organelles, including mitochondria and ribosomes (Johnstone 1992; Merryweather-Clarke 2011). The erythroid terminal differentiation occurs in anatomic niches known as the erythroblastic island (EBI), which consists of a central macrophage that plays a crucial role in erythroid differentiation by secreting growth factors to promote erythroblast proliferation and differentiation, as well as supporting their maturation by providing iron and phagocytosing expelled nuclei (Chasis 2008).

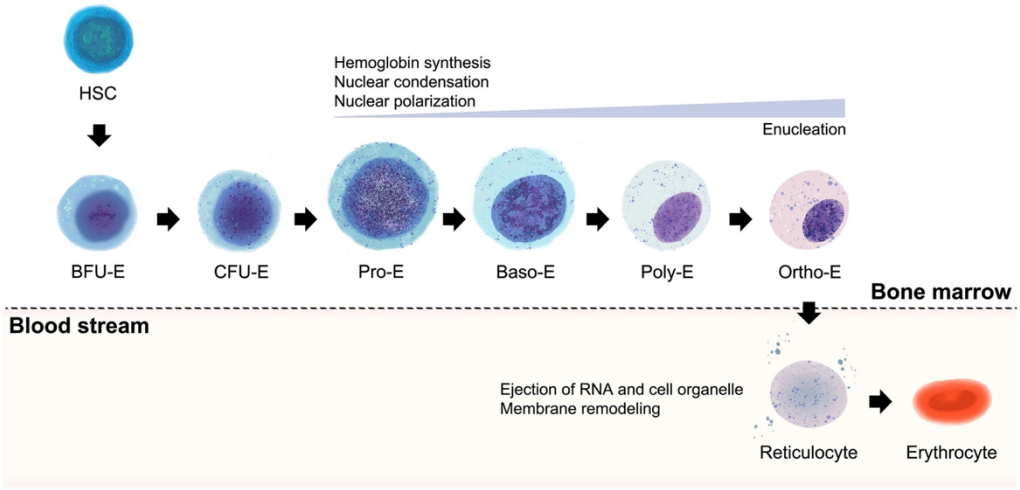

Figure 1.1: Stages of Erythroid Maturation. Progressive stages of erythroid differentiation, illustrating the relative sizes and morphologic features of hematopoietic cells at each stage. Key events include hemoglobin synthesis, nuclear condensation, and enucleation. Reticulocytes enter the bloodstream, eject organelles, and mature into erythrocytes optimized for oxygen transport. (adapted from Han 2023).

Erythropoiesis is orchestrated by a complex network of cellular factors that act synergistically or at distinct stages to ensure the effective production of RBCs. Among these, the principal regulator of this process is erythropoietin (EPO), a heavily glycosylated protein mainly produced in the kidney under hypoxic conditions. EPO exerts its regulatory effects by binding to and activating its receptor (EpoR), a single transmembrane domain expressed on the surface of immature erythroid progenitor cells that dimerizes upon ligand activation (Shih 2018). Activation of the EPO-EpoR axis triggers the JAK2/STAT5, PI3K/Akt, and MAPK signaling pathways, which collectively promote cell survival, proliferation, and differentiation (Tóthováet 2021). Additionally, transcription factors such as GATA1 and KLF1, along with cytokines including insulin-like growth factor 1 (IGF-1), interleukin-3 (IL-3), and stem cell factor (SCF), are crucial in erythroid differentiation. GATA1, the master regulator of erythropoiesis, is a zinc finger transcription factor that regulates critical processes such as globin expression, heme biosynthesis, cell cycle control, and autophagy (Ferreira 2005). Its expression is tightly controlled during

hematopoiesis, peaking in colony-forming units-erythroid (CFU-E) and proerythroblasts before declining during terminal erythroid maturation. It interacts with FOG-1 and the SCL/TAL1 complex cofactors to drive lineage-specific transcription, repress alternative hematopoietic programs, and maintain cellular fate plasticity (Gutiérrez 2020). Moreover, GATA1 directly regulates *KLF1* expression by binding to its promoter and cooperating to activate erythroid-specific genes. KLF1 is essential for Hb switching from γ- to β-globin and facilitates chromatin remodeling and transcriptional activation at erythroid loci by recruiting complexes such as CBP/p300 and SWI/SNF (Zhou 2010; Siatecka 2011). This dynamic regulation ensures a consistent oxygen supply to peripheral tissues and maintains stable Hb levels, adapting to normal and stressful conditions like hypoxia. However, when these pathways are disrupted, erythropoiesis may become ineffective, leading to conditions such as dyserythropoiesis. This phenomenon, first described by Crookston (1966), refers to an abnormal erythropoiesis process characterized by defective differentiation and proliferation pathways of the erythroid lineage, leading to impaired RBC production. It occurs in various diseases, embracing several conditions that primarily affect the nucleus or the cytoplasm of the erythroblasts. Dyserythropoiesis could be a physiological condition (e.g., during the neonatal period) or a disease (acquired or hereditary) (Iolascon 2011). This condition has been associated with a wide range of anemias, including myelodysplastic syndromes (MDS), thalassemias, and congenital dyserythropoietic anemias (CDAs). More recently, dyserythropoiesis has also been linked to pyruvate kinase deficiency (PKD), sickle cell disease (SCD), and dehydrated hereditary stomatocytosis (DHS) (Zaninoni 2023; Park 2020; Ma 2021).

1.2 Iron dysmetabolism due to chronic ineffective erythropoiesis

Iron homeostasis and erythropoiesis are tightly interconnected (Figure 1.2). Iron is essential to all hematopoietic cells, especially erythroid cells that utilize more than 80% of serum iron to synthesize the Hb needed for the daily production of about 200 billion RBC. The erythroid acquisition of iron is primarily mediated by transferrin receptor 1 (TfR1), whose expression aligns with erythroid progenitor maturation. Under physiological conditions, iron circulates predominantly between the erythron and iron-recycling macrophages. In this process, EPO plays a crucial role by stimulating the production of erythroferrone (ERFE), an erythroid-derived hormone that downregulates the SMAD signaling and hepcidin expression by sequestering BMP ligands, mainly BMP6 (Wang 2020). Hepcidin, a 25-amino acid peptide mainly produced by hepatocytes, is the master regulator of iron homeostasis. It functions by lowering serum iron levels and inhibiting ferroportin-mediated iron export from macrophages and enterocytes into the bloodstream (Nemeth 2004). During hypoxia-induced stress erythropoiesis, ERFE-mediated hepcidin suppression enhances iron efflux from macrophages and dietary iron absorption, ensuring adequate iron availability (Camaschella 2016). However, dysregulation of this mechanism can lead to systemic iron dysmetabolism and overload (Muckenthaler 2017; Kautz 2014). In inherited anemias with ineffective erythropoiesis, such as β-thalassemia and CDA II, ERFE overexpression has been identified as a key driver of pathological hepcidin suppression, leading to systemic iron overload (Kautz 2015; Russo 2016). Additionally, a rare missense variant in ERFE (ERFE-A260S) has been implicated in modifying the severity of iron overload in CDA II by disrupting hepatic iron regulation pathways (Andolfo 2019). Growth differentiation factor 15 (GDF15) and growth differentiation factor 11 (GDF11), members of the TGFβ superfamily, have also been shown to contribute to hepcidin suppression in iron-loading anemias. GDF15 is overexpressed in conditions such as thalassemia, CDA I, and CDA II, while GDF11 has been linked to beta-thalassemia, MDS, and CDA II (Casanovas

2013; Tamary 2008; Tanno 2007). Therapies targeting these pathways, such as RAP-011, a ligand trap for GDF11, are being explored as potential treatments for managing iron overload in CDA II (De Rosa 2020). Recently, fibrinogen-like protein 1 (FGL1), also known as hepassocin, has emerged as a novel erythroid regulator produced by hepatocytes in response to hypoxia. FGL1 suppresses hepcidin by binding BMP6, a mechanism demonstrated both *in vitro* and *in vivo* in male mice (Silvestri 2024). Unlike ERFE, FGL1 is not an EPO-target gene; rather, it is induced by hypoxia through two hypoxia-inducible factor binding sites in its promoter region. During anemia, the physiological response to hypoxia involves increased EPO production by the kidney, ERFE production by bone marrow and spleen, and upregulation of FGL1 and TMPRSS6 in hepatocytes (Lakhal 2011) (Figure 1.3). Although the role of FGL1 in the pathophysiology of iron-loading anemias requires further investigation, targeting FGL1 or interfering with its activity presents a potential novel therapeutic possibility for managing these conditions.

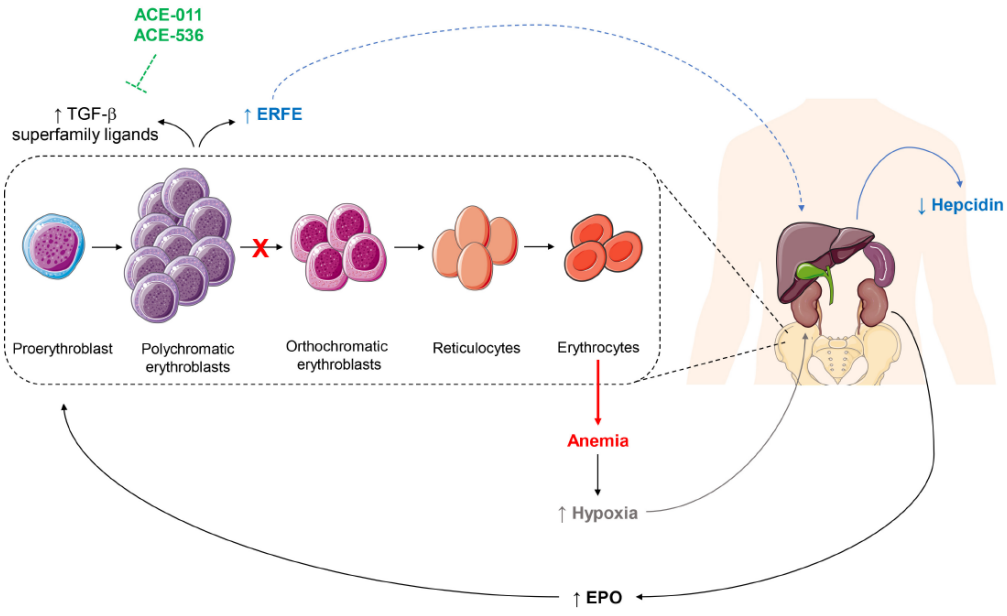

Figure 1.2: Schematic representation of the pathogenic mechanisms of CDAII at the systemic level. The pathogenic mechanism of CDAII at a systemic level highlights the role of ERFE in the interplay between the bone marrow and hepatic compartments. At the bone marrow level, the block of erythroid maturation results in the accumulation of erythroblasts that secrete ERFE. The increased levels of ERFE are responsible for the suppression of *HAMP* expression,

which encodes for hepcidin, and this can result in liver iron overload. EPO, erythropoietin; TGF-β, transforming growth factor-β (adapted from Iolascon 2020)

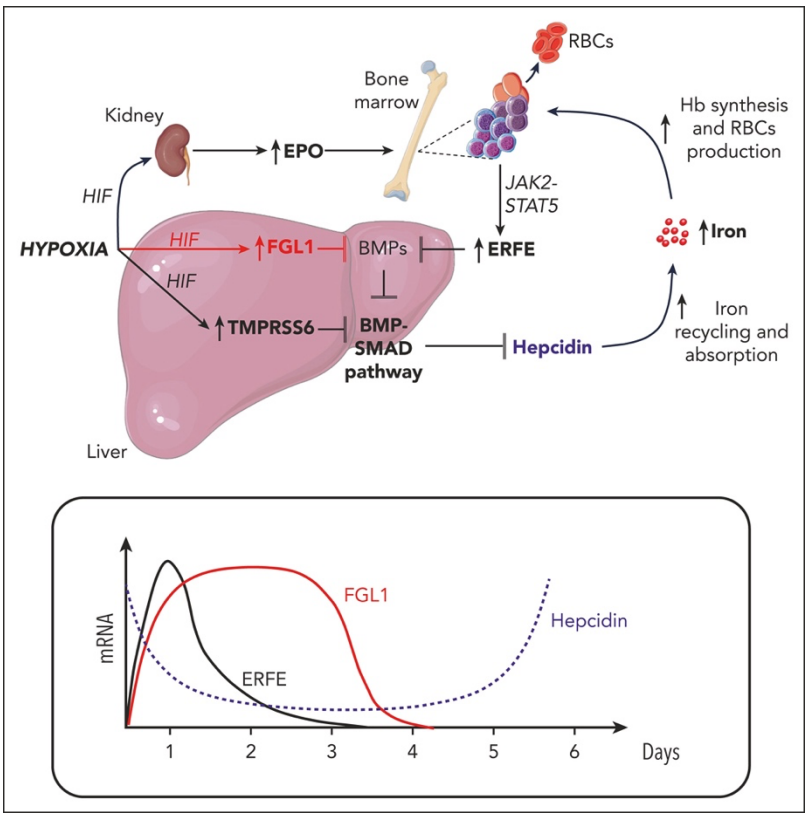

Figure 1.3: Schematic representation of ERFE and FGL1 regulation during hypoxia for hepcidin suppression and enhanced red blood cell production. Under hypoxia, EPO from the kidney stimulates RBC production, while the liver decreases hepcidin by upregulating TMPRSS6 and producing ERFE and FGL1. ERFE (peaking within 24 hours) and FGL1 (peaking after 1–3 days) inhibit BMP-SMAD signaling by sequestering BMP6, ensuring efficient hepcidin suppression. This facilitates iron recycling and absorption, providing iron for Hb synthesis and RBC production. EPO, erythropoietin; ERFE, erythroferrone; FGL1, fibrinogen-like protein 1; BMP, bone morphogenetic protein; SMAD, signaling proteins; HIF, hypoxia-inducible factor (adapted from Silvestri 2024).

1.3 Hereditary dyserythropoietic anemias: classification, diagnostic criteria, and clinical management

1.3.1 *Congenital dyserythropoietic anemias*

Congenital dyserythropoietic anemias (CDAs) are a large group of hypo-productive anemias that result from various kinds of abnormalities during the late stages of erythropoiesis (Russo 2020). They are classified as inherited BM failure syndromes, marked by distinct morphological abnormalities in BM erythroblasts and ineffective erythropoiesis as the main cause of anemia, often accompanied by a hemolytic component (Iolascon 2013). Clinically, patients with CDAs typically present with anemia and hemolytic signs, accompanied by reticulocytosis inadequate to the degree of anemia. The diagnostic criteria for CDAs include (1) the presence of anemia, jaundice, and splenomegaly; (2) evidence of ineffective erythropoiesis; (3) specific morphological abnormalities in erythroblasts observed in BM examinations; and (4) exclusion of other congenital anemias that satisfy criteria 1 and 2, such as thalassemia syndromes and other inherited BM failure disorders. In the last two decades, many advances have been made in understanding CDAs, particularly with the identification of the causative genes that helped to investigate the molecular basis of CDAs and to unravel novel aspects of the molecular biology of erythropoiesis (Gambale 2016). Currently, CDAs are classified into three main subtypes (CDA I, II, and III) based on BM morphological abnormalities (Iolascon 2012) (Figure 1.4). Additionally, non-conventional variants have also been identified, which can be classified as transcription-factor-related CDAs, CDA variants, and syndromic CDAs (Table 1) (Russo 2024). Thanks to the development of high-throughput technologies such as next-generation sequencing (NGS), the list of causative genes is continuously updated. Most of these conditions show a monogenic inheritance pattern, but emerging evidence suggests that some cases of CDAs may involve complex modes of inheritance. This includes the co-inheritance of genetic modifiers that can influence disease severity or phenotype, as well as digenic or dual inheritance patterns that involve simultaneous mutations in

distinct genes (Andolfo 2021). The main complications of CDAs are linked to chronic hemolytic anemia, which is associated with hyperbilirubinemia, gallstones, and splenomegaly. The most harmful issue in CDAs is iron overload, primarily driven by ineffective erythropoiesis (Figure 1.2) and further exacerbated by transfusion regimen and the hemolytic component of the disease. Severe iron overload in CDA patients can lead to liver damage, heart failure, diabetes, and hypogonadotropic hypogonadism, which are often correlated with subfertility and osteopenia. Clinical management depends on the severity of symptoms and includes transfusions for severe anemia and iron chelation therapy to mitigate iron overload. Periodical evaluation of the iron balance parameters in the serum, such as ferritin, transferrin saturation, and hepcidin, as well as the assessment of iron accumulation in the liver and heart using T2*-weighted magnetic resonance, are crucial to monitor patients. Splenectomy may be considered for patients with symptomatic splenomegaly, but its use is restricted to selected cases due to potential risks (Iolascon 2020). Recent therapeutic advances have focused on targeting ineffective erythropoiesis, while emerging approaches, such as hematopoietic stem cell transplantation and gene therapy, are under investigation, even though they are still far from routine clinical practice (Ayas 2002; Miano 2019; Nair 2009).

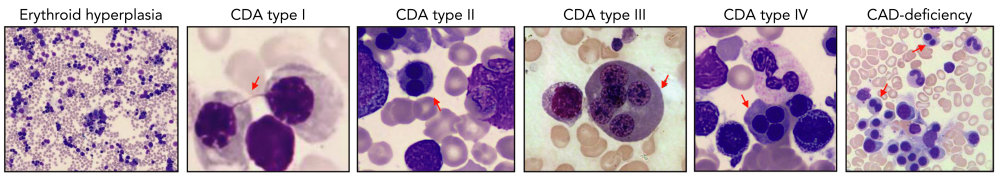

Figure 1.4: Morphological and molecular characteristics of CDA patients. Light microscopy analysis of bone marrow samples from patients with various CDA subtypes. CDA is generally characterized by erythroid hyperplasia. Red arrows highlight distinctive features of each subtype: CDA I, internuclear chromatin bridges; CDA II, binucleated erythroid precursors (adapted from Iolascon 2020).

Table 1. Classification of hereditary dyserythropoietic anemias

Disease symbol	***Gene*** Location	**Inheritance**	**Phenotype MIM number[§]**	**Main clinical and laboratory features**	**Bone marrow morphological features**
Classical forms of CDAs					
CDA Ia	*CDAN1* 15q15.2	AR	224120	Anemia typically of moderate severity (Hb 8-10 g/dL), often macrocytic. Dysmorphic features present in 4-14% of individuals: syndactyly, phalangeal hypoplasia, extra metatarsal bones, clubfoot, short stature, thoracic dysplasia, short limbs.	Erythroid hyperplasia with binucleate polychromatic erythroblasts (3–7%); thin chromatin bridges between nuclei of erythroblasts (1.4–7.9%). EM: spongy heterochromatin (or "Swiss cheese appearance") in up to 60% of early and late polychromatic erythroblasts.
CDA Ib	*CDIN1* 15q14	AR	615631		
CDA II	*SEC23B* 20p11.23	AR	224100	Anemia of variable degree, usually moderate (Hb 8-10 g/dL) and normocytic/slightly macrocytic. Hypoglycosylation of the erythrocyte protein band 3.	Binucleated intermediate/late erythroblasts (10–30%); rare multinucleated erythroblasts. Karyorrhexis; Gaucher-like cells in ~ 60% of patients. EM: double plasma membrane of the erythroblasts.
CDA IIIa	*KIF23* 15q23	AD	105600	Anemia typically mild or absent. Macrocytosis and poikilocytosis. Hemolysis, jaundice, and cholelithiasis are common. Serum thymidine kinase is markedly increased. Co-occurrence of myeloma and monoclonal gammopathy.	Giant multinucleated (up to 12 nuclei) in 16–23% of marrow erythroblasts. EM: clefts within heterochromatin, autophagic vacuoles, iron-laden mitochondria, myelin figures in the cytoplasm.
CDA IIIb	*RACGAP1* 12q13.12	AR	619789	Moderate-to-severe macrocytic anemia and hepatosplenomegaly.	Multinucleated erythroblasts and gigantoblasts.
Transcription factors-related CDAs					
CDA IV	*KLF1* 19p13.13	AD	613673	Hemolytic anemia generally severe, with normal or slightly increased reticulocyte count, and markedly elevated fetal hemoglobin levels.	Bi/tri-nucleated erythroblasts. EM: immature erythroid progenitors with atypical cytoplasmic inclusions, invagination of the nuclear membrane, and marked heterochromatin
XLTDA	*GATA1* Xp11.23	XLR	300367	Macro-thrombocytopenia, bleeding tendency, and mild-to-severe anemia	Erythroblasts with megaloblastic features, bi- and multi-nucleation, and nuclear irregularities; small dysplastic megakaryocytes with signs of incomplete maturation and reduced number of alpha granules

Table 1. Classification of hereditary dyserythropoietic anemias (*continued*)

Disease symbol	*Gene* Location	Inheritance	Phenotype MIM number[§]	Main clinical and laboratory features	Bone marrow morphological features
CDA variants					
-	*ALAS2* Xp11.21	XLD	-	Macrocytic anemia with iron overload in female individuals.	Erythroid hyperplasia with dyserythropoiesis; rare erythroblasts with siderotic granules (no excess iron or sideroblasts).
MEVA	*MVK* 12q24.11	AR	610377	Mevalonate kinase deficiency associated with CDA II-like anemia.	CDA II-like morphological abnormalities of erythroblasts.
PKD	*PKLR* 1q22	AR	266200	Pyruvate kinase deficiency often misdiagnosed as CDA I or II in transfusion-dependent patients.	CDA I-like morphological abnormalities of erythroblasts.
DHS1	*PIEZO1* 16q24.3	AD	194380	Hemolytic anemia, mild to moderate with elevated MCV. Dehydrated RBCs (reduced osmotic fragility) and altered RBC cation content (↑Na+, ↓K+). Hyperbilirubinemia and Splenomegaly (variable).	Erythroid hyperplasia (increased erythroid precursors). Dyserythropoiesis (irregularly shaped erythroid precursors). No significant fibrosis or structural abnormalities.
Syndromic CDAs					
MJDS	*LPIN2* 18p11.31	AR	609628	Hypochromic microcytic anemia; chronic recurrent multifocal osteomyelitis and inflammatory dermatosis.	Microcytosis and dyserythropoiesis.
EIEE50	*CAD* 2p23.3	AR	616457	Autism, developmental delay, and generalized epilepsy; mild CDA II-like anemia with marked anisopoikilocytosis and abnormal glycosylation of the erythrocyte proteins band-3 and RhAG.	Erythroid hyperplasia with dyserythropoiesis, bi- and tri-nucleated erythroblasts, prominent cytoplasmic bridging.
CIMDAG	*VPS4A* 16q22.1	AD (*de novo*)	619273	Microcephaly, hypotonia, global developmental delay, structural brain abnormalities, cataracts; hemolytic anemia.	Dyserythropoiesis with 3-7% binucleated erythroblasts and cytoplasmic bridges.

[§]Phenotypes exclusively associated with dyserythropoiesis were reported.
AR, autosomal recessive; AD, autosomal dominant; XLR, X-linked recessive; XLD, X-linked dominant; EM, electron microscopy.
CDA, congenital dyserythropoietic anemia; CDA I, CDA type I; CDA II, CDA type II, CDA III, CDA type III; CDA IV, CDA type IV; XLTDA, X-linked thrombocytopenia with or without dyserythropoietic anemia; MEVA, mevalonic aciduria; PKD, pyruvate kinase deficiency; MJDS, Majeed syndrome; EIEE50, early infantile epileptic encephalopathy-50; CIMDAG, cerebellar hypoplasia-intellectual disability-congenital microcephaly-dystonia-anemia-growth retardation syndrome. (adapted from Russo 2024)-

1.3.2 CDA type I

CDA I is characterized by moderate-to-severe macrocytic anemia, which can manifest in utero as severe anemia associated with hydrops fetalis or, more commonly, after birth with symptoms such as hepatomegaly, early jaundice, and intrauterine growth restriction (Kato 2001; Roy 2019). Beyond the neonatal period, affected individuals typically experience lifelong moderate anemia, often

with a normal mean corpuscular volume (MCV) and marked reticulocytopenia. All patients develop splenomegaly in adolescence or adulthood, while about 20% of cases present congenital anomalies, particularly syndactyly in hands or feet, absence of nails or supernumerary toes, pigeon chest deformity, and short stature (Iolascon 2012; Gambale 2016). In the bone marrow, 2.4% to 10% of late erythroblasts are binucleate, most of which have nuclei at different stages of erythroid differentiation. The hallmark morphological feature of CDA I is the presence of thin internuclear chromatin bridges between nuclear pairs of intermediate erythroblasts, observed in 79% of CDA I patients. Transmission electron microscopy (TEM) reveals denser heterochromatin forming clumps with small translucent vacuoles, giving a "Swiss cheese" appearance in up to 60% of early and late polychromatic erythroblasts (Heimpel 2010). CDA I estimated frequency is ~1:207.000 live births (Olijnik 2021). It is an autosomal recessive disease caused by loss-of-function mutations in *CDAN1* (CDA Ia) or *CDIN1* (CDA Ib), accounting for ~80% and ~10% of the disease, respectively. Despite being widely expressed, mutations in these genes primarily affect the erythroid lineage, possibly due to the uniquely fast cell cycle of erythroid progenitors or the requirement for histone eviction, such as H3 and H4, during nuclear extrusion in erythroblasts, a process in which they are likely functionally implicated (Roy 2019). To date, 90 causative mutations have been documented, with only 10 of them in *CDIN1* (Babbs 2013; Marra 2024). Nevertheless, the remaining ~10% of patients may have mutations in noncoding regulatory elements of *CDAN1* or *CDIN1* or in yet unidentified CDA I-causing genes. CDA Ib patients appear to be more severely affected compared to CDA Ia patients, as evidenced by the predominance of transfusion dependence in most described cases (Gambale 2016). Nonetheless, differences in Hb and MCV values can aid in distinguishing between them. Patients with CDA I may benefit from interferon-α (IFN-α) therapy, which can improve Hb levels and reduce iron overload. The mechanism underlying this response remains unknown. To date, only a limited number of individuals, including infants, have been treated,

showing highly variable responses. For those who are transfusion-dependent and unresponsive to IFN-α, allogeneic bone marrow transplantation remains a potential option (Lavabre-Bertrand 1995; Tamary 2021).

1.3.3 CDAN1

CDAN1, located on chromosome 15q15.2, was the first gene in which pathogenic variants were identified (Dgany 2002). It is a 28-exon gene that is ubiquitously expressed and encodes a 134 kDa protein, referred to as codanin-1. Recent analyses have identified no mutational hotspots in *CDAN1*, with pathogenic variants distributed across the gene, including frameshift, missense, and truncating mutations (Marra 2024) (Figure 1.5). Codanin-1 is a highly conserved nuclear protein, predominantly localized in the nuclear heterochromatin and regulated by the cell cycle. During mitosis, codanin-1 undergoes phosphorylation, causing its exclusion from condensed chromosomes. Its transcription is regulated by E2F1, a key regulator of the G1/S transition, which binds to the *CDAN1* promoter during the S phase to elevate codanin-1 levels (Noy-Lotan 2009). It is part of the cytosolic Asf1-H3-H4-importin-4 complex, where it sequesters multiple Asf1 molecules via two H3 mimic helices (HMHA1 and HMHA2) and two B domains (BDA1 and BDA2), inhibiting their chaperone function (Sedor 2024). Once codanin-1 dissociates, Asf1 can interact with histone chaperones to facilitate chromatin assembly. *CDAN1* mutations disrupt this process, causing abnormal Asf1 accumulation on chromatin, uncontrolled DNA synthesis, and failure to regulate critical checkpoints in chromatin replication (Ask 2012). Recent studies on human umbilical cord blood-derived erythroid progenitors (HUDEP-2), mutated for two common heterozygous *CDAN1* variants, have shown decreased cell viability and increased intercellular bridging and binucleation, indicating cellular instability. These mutations also disrupt histone availability and acetylation, leading to cell cycle disruptions and impairing terminal erythroid maturation (Murphy 2020). Codanin-1's crucial role extends to cellular development and hematopoiesis,

particularly evident in early embryonic stages, where its absence leads to embryonic lethality in mice before the onset of hematopoiesis (Renella 2011). Of note, a completely null genotype has never been identified in a CDA I patient, suggesting that a complete absence of codanin-1 is lethal.

1.3.4 CDIN1

The second gene identified as causative of CDA Ib is *C15orf41*, located on chromosome 15q14 (Babbs 2013), recently renamed *Codanin-1 Interacting Nuclease 1* (*CDIN1*). *CDIN1* is composed of 11 exons and is widely transcribed, though its expression is notably elevated in B lymphoblasts, CD34+ cells, cardiomyocytes, and fetal liver, suggesting a specific role in hematopoiesis (Su 2004). It encodes a 32 kDa protein that is uniformly expressed during erythroid differentiation and is highly conserved across eukaryotes (Merryweather-Clarke 2011). Consistent secondary structure predictions, confirmed by profile-to-profile comparison methods, provide strong evidence that *CDIN1* contains two N-terminal AraC/XylS-like wHtH domains and a PD-(D/E)XK nuclease domain, suggesting its function as a divalent metal-ion-dependent endonuclease involved in DNA damage repair, Holliday junction resolution, recombination, and RNA processing. Structural studies indicate that CDIN1 protein is both thermostable and unstable, with acidic properties. It is also predicted to contain a TPD (Treponema pallidum) domain spanning residues 135 to 265, though its function remains unknown, along with three post-translational modification (PTM) sites: K50 (acetylation), T114 (phosphorylation), and K176 (ubiquitination) (Figure 1.5) (Ahmed 2018). Recent studies have shown that CDIN1 forms a stable complex with Codanin-1 via its C-terminal region, underscoring their close relationship and supporting the hypothesis of a functional connection between these proteins in the pathogenesis of CDA I. Although CDIN1 is found in both the cytosol and the nucleus/nucleolus, its interaction with codanin-1 confines it primarily to the cytosol, suggesting that CDAN1 regulates CDIN1's localization and prevents its nuclear entry, where it

might otherwise participate in nuclease-related activities (Shroff 2020; Swickley 2020). CDIN1 has also been shown to interact with Asf1b, the paralog of Asf1a, further supporting the notion that the primary defect in CDA I may involve disruptions in DNA replication and chromatin assembly. Recent studies on CD34+ cells from CDA-I patients have revealed delayed erythroid differentiation accompanied by nucleolar disorganization and reduced ribosomal RNA synthesis, underscoring the role of nucleolar dysfunction in CDA-I pathogenesis (Scott 2021). Moreover, functional studies revealed that mutations such as Y94S, H230P, and P20T in *CDIN1* impair erythroid maturation, disrupt S-phase progression, and significantly reduce $CD71^{+}/CD235^{+}$ cells, indicating impaired erythroid differentiation. These mutations are also associated with defective nucleosome assembly and altered transcriptional regulation, highlighting the critical role of chromatin dynamics and cell cycle dysregulation in the pathogenesis of CDA I (Russo 2019; Marra 2024).

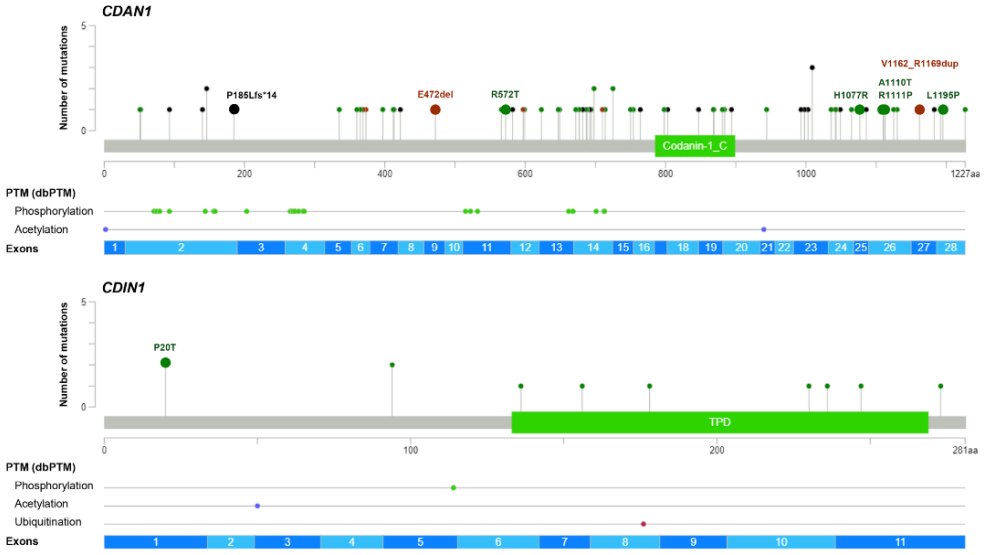

Figure 1.5: Schematic representation of *CDAN1* and *CDIN1* and localization of known coding pathogenic variants. (Upper panel) CDAN1 linear protein is shown with its domains, exons, and Post Translational Modification (PTM) sites. The lollipop plot shows 80 pathogenic variants, with 72 variants already reported in the HGMD database (HGMD professional 2023.4), and the 8 newly identified variants (big circles). **(Lower panel)** CDIN1 linear protein with its domains, exons, and PTM sites is shown. The lollipop plot shows 10 pathogenic variants, with the c.58C > A, p. Pro20Thr newly identified variant (big circle). Missense variants are shown in

green, in frame variants in brown, and truncating variants in black. The exons are numbered to show the location of each mutation (adapted from Marra 2024).

1.3.5 CDA type II

CDA type II, the most prevalent form of congenital dyserythropoietic anemias, is an autosomal recessive disorder caused by biallelic mutations in the SEC23B gene (chr 20p11.23) (Schwarz 2009). It typically manifests as moderate to severe normocytic or microcytic anemia, often accompanied by normal or slightly elevated reticulocyte counts. Common clinical features include jaundice, splenomegaly, and gallstones, largely attributed to the hemolytic component of the disease. Although most CDA II patients are mildly affected, clinical severity varies widely, with approximately 10% of cases being asymptomatic and 20% requiring regular blood transfusions. The primary complications in CDA II arise from disruptions in iron homeostasis, driven by ineffective erythropoiesis and further exacerbated by hemolysis and transfusion dependency (Gambale 2016). Elevated levels of GDF15 and ERFE, along with a specific hepatic role of *SEC23B*, contribute to systemic iron overload. Emerging treatments for CDA II, such as luspatercept and sotatercept (activin receptor ligand traps), are being investigated (Cappellini 2019). These therapies, already approved for β-thalassemia, target ineffective erythropoiesis by blocking TGF-β superfamily ligands and inhibiting the SMAD2/3 signaling pathway. Preclinical studies with RAP-011, a murine analog of sotatercept, have demonstrated the potential to restore erythroid gene expression and reduce ERFE levels in CDA II models, providing a promising therapeutic avenue (De Rosa 2020). In the BM, CDA II is characterized by hypercellularity, pronounced erythroid hyperplasia, and a distinct presence of binucleated erythroblasts, with nuclei at the same maturation stage, involving up to 10% of erythroblasts. Under TEM, mature erythroblasts display a discontinuous “double membrane” attributed to vesicles loaded with endoplasmic reticulum (ER) proteins positioned beneath the plasma membrane. Additionally, a pathognomonic biochemical marker of CDA II is the presence of

glycosylation abnormalities in the fast-moving band 3 (anion exchanger 1) and band 4.5 (glucose transporter 1) proteins, observed in 95% of cases.

1.3.6 SEC23B

SEC23B encodes a key component of the cytoplasmic coat protein complex II (COPII), essential for anterograde vesicle trafficking of properly folded proteins from the endoplasmic reticulum (ER) to the Golgi apparatus (Russo 2013; Schwarz 2009). Specifically, SEC23B functions as a GTPase-activating protein (GAP) for SAR1, a small GTPase that initiates vesicle formation on the ER membrane. Together with SEC24, SEC23B forms the inner layer of the COPII coat, capturing specific cargo and facilitating vesicle budding. Activated SAR1 binds to the ER membrane, recruiting the SEC23/SEC24 heterodimer to form the "pre-budding" complex, which in turn recruits SEC13/SEC31 to form the outer COPII coat. This outer layer stabilizes the vesicle structure, allowing the transport of various cargo sizes (Figure 1.6). Despite its ubiquitous expression, SEC23B mutations predominantly affect the erythroid lineage. This specificity may result from the tissue-restricted expression of *SEC23B* during erythroid differentiation or from the unique transport demands of erythroid-specific cargoes, such as band 3, which likely require high levels and full functionality of COPII components (Russo 2013). Furthermore, SEC23B may play a crucial role in midbody assembly or disassembly, with its loss of function potentially contributing to the impaired cytokinesis observed in CDA II erythroblasts (Gambale 2016). Additional studies have also highlighted SEC23B's involvement in promoting autophagic flux, a process essential for the final stage of reticulocyte maturation (Ishihara 2001). Moreover, SEC23B plays a critical role in liver homeostasis by regulating systemic iron levels through the BMP/SMAD signaling pathway (Figure 1.7). Loss of SEC23B function in hepatic cells disrupts the glycosylation and membrane localization of key BMP6 signaling components, such as HFE, TFR2, and HJV. This impairment led to decreased SMAD1/5/8 phosphorylation and

suppressed hepcidin transcription, contributing to the iron overload characteristic of CDA II patients independently of erythroferrone regulation (Rosato 2022). Understanding the pathophysiology of CDA II is difficult, primarily due to the lack of a reliable animal model. Sec23b-deficient mice die shortly after birth from pancreatic degeneration, and tissue-specific knockouts do not exhibit CDA II characteristics because of the compensatory expression of SEC23A (Tao 2012; Khoriaty 2016). Currently, a *SEC23B* knockout model in HUDEP-2 cells has been developed, demonstrating CDA II-like features, such as reduced cell viability, impaired expansion, and increased binuclearity upon differentiation. Remarkably, reintroducing *SEC23A* rescues these defects, underscoring the compensatory potential of *SEC23A* and the value of this model for studying CDA II pathogenesis and exploring therapeutic strategies (King 2021).

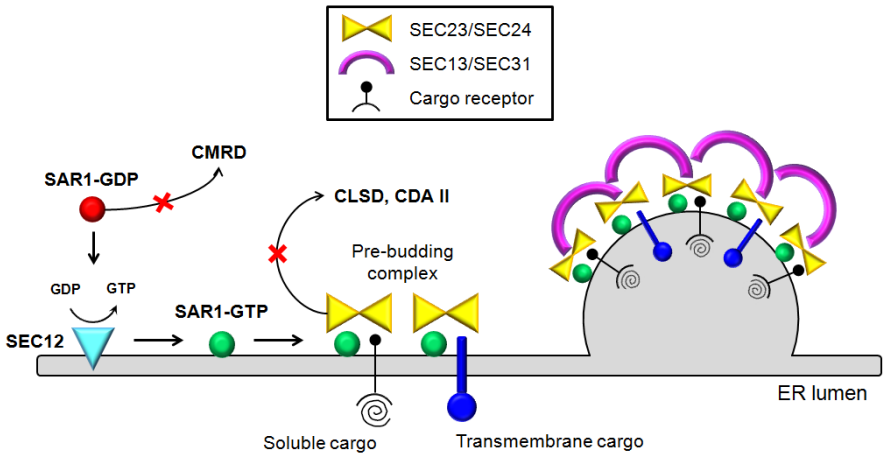

Figure 1.6. Recruitment mechanism of COPII. COPII-coated vesicles form by the sequential binding of Sar1-GTP, the inner complex proteins Sec23- Sec24, and the outer complex components Sec13-Sec31 on the endoplasmic reticulum. The transport of both integral membrane cargo and soluble secretory cargo is shown (adapted from Russo 2013).

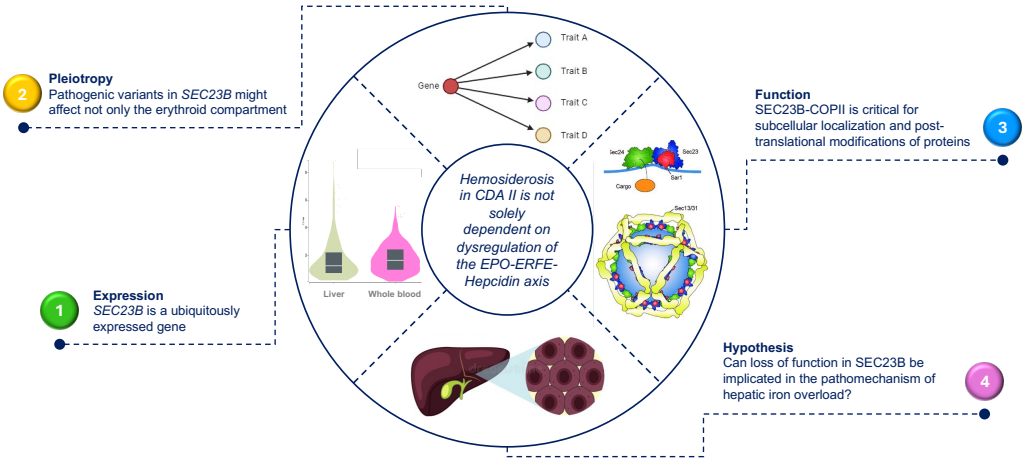

Figure 1.7: Schematic representation of the molecular and cellular mechanisms associated with SEC23B function. This figure highlights its ubiquitous expression, the pleiotropic effects of its pathogenic variants, the critical role of SEC23B-COPII in subcellular localization and post-translational protein modifications, and its involvement in hepatic iron overload, which is not solely dependent on dysregulation of the EPO-ERFE-hepcidin axis.

1.3.7 Dehydrated Hereditary Stomatocytosis

Dehydrated hereditary stomatocytosis (DHS), also known as xerocytosis, is an autosomal dominant hereditary hemolytic anemia characterized by increased permeability of RBC membrane to monovalent cations Na+ and K+, with the consequent changes to intracellular cation content and cell volume. The prevalence of DHS is not yet well established, as many cases are likely undiagnosed or misclassified under other hemolytic disorders. DHS1 patients' phenotype ranges from asymptomatic to severe hemolytic forms (Da Costa 2013) and may occur as an isolated condition or, more commonly, as part of a syndrome with pseudohyperkalemia and/or perinatal edema (Grootenboer 2000). It typically presents as hemolytic well-compensated anemia, with a high reticulocyte count, a tendency to macrocytosis, and mild jaundice. The major complications of DHS are splenomegaly, resulting from increased red cell trapping in the spleen, and cholelithiasis due to elevated bilirubin levels (Andolfo 2016). However, splenectomy is contraindicated because of the risk of severe thrombotic events (Iolascon 2017). Notably, DHS patients also tend to have iron overload, which frequently leads to hepatosiderosis (Syfuss 2006;

Badens 2016; Orvain 2018; Andolfo 2018). In blood smears, these patients show rare stomatocytes, erythrocytes with a characteristic central mouth-shaped slit, represented by a linear unstained area across their center. Osmotic gradient ektacytometry is considered the "gold standard" for the diagnosis of this condition, which shows a specific curve with a leftward shift of the minimum in the deformability index (Omin) at low osmolarities, as well as a decrease in the maximum deformability index (DImax) (Figure 1.8). DHS is caused by mutations at two different loci: (i) *PIEZO1* (16q24.3) for DHS type 1 (DHS1) and (ii) *KCNN4* (19q13.31) for DHS type 2 (DHS2) or Gardos Channelopathy (Zarychanski; Andolfo 2013; Rapetti-Mauss 2015). The two forms of DHS showed very similar phenotypes, even if some differences can be observed. DHS2 patients are more severely anemic than DHS1 one (Andolfo 2018a; Andolfo 2018b).

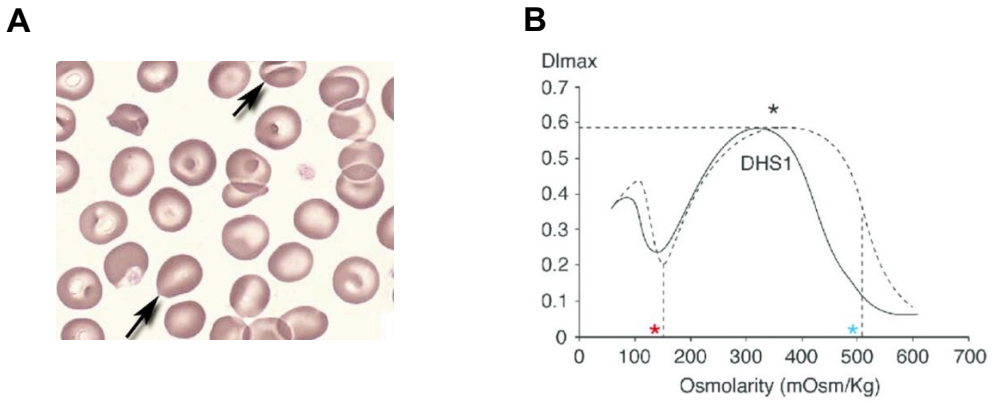

Figure 1.8: Morphological and rheological features of erythrocytes from DHS patients. A. Stomatocytes are highlighted on a blood smear (black arrow) (adapted from Da Costa 2013) **B**. Osmotic gradient ektacytometry on a DHS patient (continuous curve), left-shifted respect of healthy control (dashed curve). Parameters of interest are signed: Omin point (red asterisk); the maximal deformability index (DImax, black asterisk); O′ or hyper point (blue asterisk) (adapted from Andolfo 2016).

1.3.8 PIEZO1

PIEZO1 was the first gene identified as causative for DHS1 through exome sequencing (Zarychanski 2012; Andolfo 2013). It encodes a mechanoreceptor functioning as a cation-selective channel activated by mechanical force, allowing the passage of both monovalent and divalent cations (Coste 2012; Kim 2012; Gnanasambandam 2015). PIEZO1, one of the largest ion channels identified to date, forms a trimeric propeller-like structure with three curved "blades" surrounding a central pore and a cap, termed the C-terminal extracellular domain (CED), which, together with the outer and inner helices, forms the permeation pathway (Figure 1.9). Several missense variants have been reported, primarily in the highly conserved C-terminal regions encoding the pore domain responsible for ion conduction and selectivity (Andolfo 2018). Notably, patients with pathogenic variants in the pore domain exhibit more severe phenotypes than those with variants in non-pore regions, which influence the mechanosensitive properties of the channel. *PIEZO1* mutations have also been linked to severe iron overload, suggesting a role for this mechanoreceptor in iron metabolism regulation. Although iron overload was initially believed to occur independently of erythroid involvement (Orvain 2018), recent studies have demonstrated that *PIEZO1* activation disrupts erythroid progenitor proliferation and differentiation through transcriptional dysregulation (Caulier 2020). Furthermore, macrophage-specific gain-of-function (GoF) mutations in *PIEZO1* result in reduced hepcidin expression and elevated ERFE levels, enhancing erythropoiesis and accelerating erythrocyte turnover via increased macrophage phagocytic activity, thereby contributing to systemic iron overload (Ma 2021). Recent findings further elucidated the PIEZO1 role in iron metabolism regulation. *PIEZO1* R2456H variant in hepatic cell lines (HuH7 and HepG2) induces hyper-phosphorylation of ERK1/2, suppressing R-SMAD activation and hepcidin expression (Andolfo 2020). Specifically, multi-omics analysis of *PIEZO1* R2456H-mutant hepatic cells revealed dysregulation of the "Regulation of Actin Cytoskeleton" pathway,

implicating RAS and integrin-mediated signaling in cytoskeletal instability. Partial restoration of *HAMP* expression following inhibition of *RAS* and ERK signaling further supports the role of *PIEZO1* in MAPK-dependent hepcidin regulation (Rosato 2024).

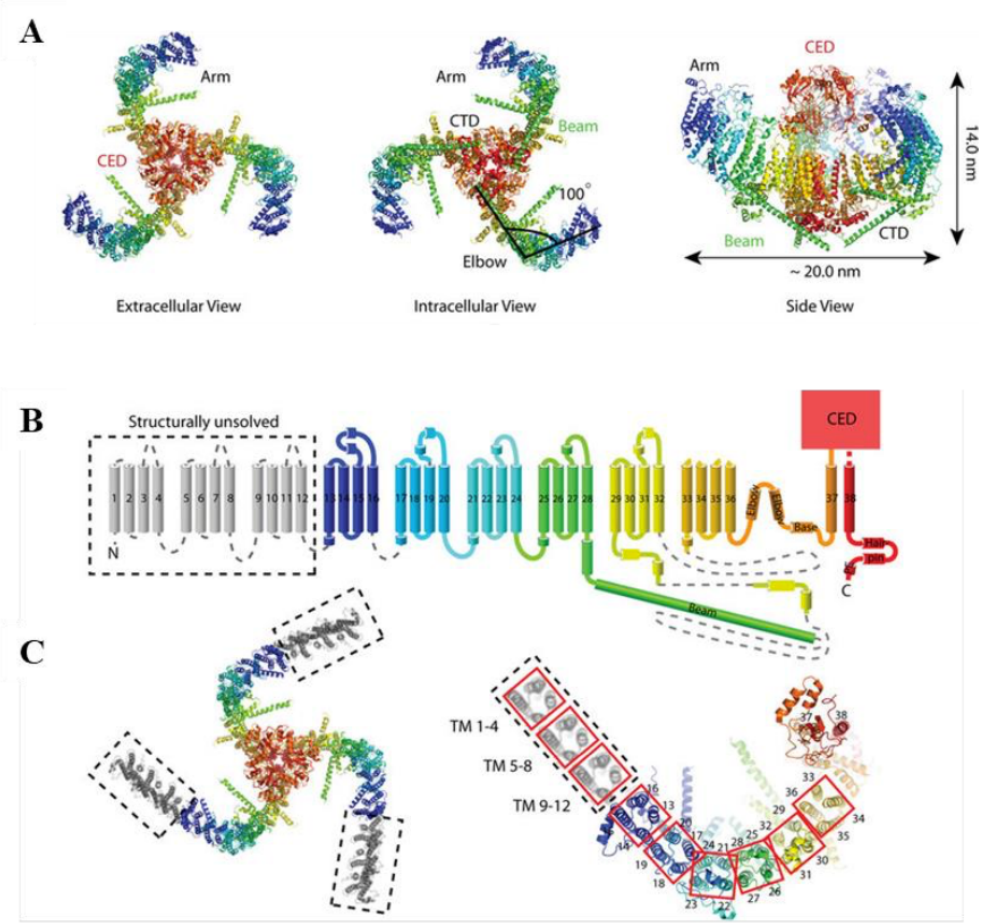

Figure 1.9: Architecture and topology of the mechanosensitive channel PIEZO1. **A.** Top, bottom, and side views of PIEZO1 in cartoon representation. **B.** Topology of PIEZO1 shown rainbow-colored (with N terminus in blue and C terminus in red), except for the structurally unsolved TM1–TM12 regions (shown in grey). Helices are represented as cylinders, loops as solid lines, and unresolved regions as dotted lines. **C**. Top view of transmembrane helices labeled as in the topology. Red squares outline four transmembrane units that constitute the arm. TM21–TM24 are at the 'elbow' of the arm. The hypothetical position of the unresolved units TM1–TM4, TM5–TM8, and TM9–TM12 are indicated (dashed outline) (adapted from Lin 2019).

2. Aim of the study

This PhD project is focused on the study of the molecular genetics and pathogenetic mechanisms underlying dyserythropoiesis and iron overload in inherited hemolytic anemias, specifically DHS1 and CDA types I and II. Although these disorders belong to different subtypes within the broader group of hereditary hemolytic anemias, i.e., RBC membrane defects and hypo-productive anemias, they share common characteristics, like impaired erythroid maturation and systemic iron overload. Despite significant advances in understanding their clinical presentations, the molecular pathways driving these conditions remain still undefined. The aims of this project are:

1. to elucidate the mechanisms of impaired erythroid differentiation and proliferation through the establishment and characterization of cellular models for CDA I, CDA II, and DHS1.

2. to characterize iron metabolism dysregulation and its clinical implications, particularly in cases with dual inheritance patterns of *SEC23B-PIEZO1* pathogenic variants.

3. Materials and Methods

3.1 Patients and genomic DNA preparation

Five hundred eighty-one patients with clinical suspicion of different types of HAs were included in the study. Clinical diagnosis was based on history, clinical findings, laboratory data, morphological analysis of peripheral blood, aspirated BM whenever available, and genetic testing. Local university ethical committees approved both the DNA sampling and the collection of patient data from the Medical Genetics Ambulatory in Naples (University Federico II, DAIMedLab). DNA and plasma samples from patients were obtained after signed informed consent and according to the Declaration of Helsinki. Genomic DNA (gDNA) preparation was performed as previously described (Russo 2013). Samples were quantified by NanoDrop spectrophotometer (Thermo Scientific, Italy). Then, gDNA was loaded on 0,8% DNA agarose gel electrophoresis to assess integrity.

3.2 Targeted NGS of HAs patients

3.2.1 Libraries establishment

Genetic testing was achieved by targeted NGS using a 124-gene custom gene panel for hereditary RBC defects, namely RedPanel_rev.3. For probe design, coding regions, 5′UTR, 3′UTR, 50 bp flanking splice junctions were selected as regions of interest. Probes were designed using the web-based tool SureDesign (https://earray.chem.agilent.com/suredesign.htm, Agilent Technologies, USA). The sequence length was set at 150 x 2 nucleotides. The total probe size was 298.393 kbp. Sample preparation was performed following the manufacturer's for SureSelectXT HS Target Enrichment for the Illumina Platform - Magnis SureSelect XT HS Rev B Reagent Kit - with Tier 1 (1–499 kb).

3.2.2 Sequencing and data analysis

High-throughput sequencing was performed by Illumina MiSeq. The alignment of sequencing reads to the genomic reference, quality control, and identification of variants were carried out using an in-house pipeline. Briefly, sequencing reads were aligned to the GRCh37/hg19 version of the human genome using the bwa-mem2 (v2.2.1) algorithm. Single nucleotide variants were annotated with Annovar (v2019-10-24), and variants were viewed and interpreted using the seqr platform (v1.0-956f348a). The pathogenicity of each variant was evaluated according to American College of Medical Genetics and Genomics (ACMG) guidelines, incorporating evidence from population data, computational predictions, functional data, and segregation data. A scaled point system was employed, attributing scores of 0 to 4 for variants of unknown significance (VUS), 5 for VUS/likely pathogenic variants (LP), 6-9 for LP, and a score equal to or greater than 10 for pathogenic variants (P). Patients with variants scoring ≥4 were considered diagnosed. Due to the large range of prevalence in the population of these heterogeneous disorders, we selected both rare and low-frequency variants (AF < 0.01 and 0.05, respectively), as reported by gnomAD browser (https://gnomad.broadinstitute.org/). For clinical interpretation, InterVar (http://wintervar.wglab.org/), Varsome (https://varsome.com/), and Franklin (https://franklin.genoox.com/clinical-db/home) were used. All prioritized variants were confirmed by Sanger sequencing and inheritance pattern analysis whenever possible. Validations were performed using 50 ng of gDNA. Custom primers were designed using Primer3 software (Primer3 v. 0.4.0).

3.3 Plasma collection and ELISA assay

Plasma samples were collected from the peripheral blood of patients and healthy controls (with informed consent, according to the Declaration of Helsinki). Plasma levels of ERFE and Hepcidin were quantified using ELISA

kits (Intrinsic Erythroferrone IE; Intrinsic Lifesciences, CA, USA, Intrinsic HEPCIDIN IDx™, Intrinsic Lifesciences, CA, USA) as previously described (Ganz 2017). The ERFE and Hepcidin levels in each sample were determined through the fitting of a four-parameter logistic curve according to the manufacturer's protocol.

3.4 Cell cultures

LentiX-293 and Hep3B cells were obtained from the American Type Culture Collection (ATCC, Manassas, VA, United States). Hep3B cells enriched for 18% in the *PIEZO1*-R2456H variant (PIEZO1-KI cells) were produced by Synthego Corporation (Synthego, Menlo Park, CA, United States). Cells were maintained in high-glucose Dulbecco's Modified Eagle's Medium (DMEM; Sigma-Aldrich) and Essential Modified Eagle's Medium (EMEM; Sigma-Aldrich) supplemented with 10% fetal bovine serum (Life Technologies), 100 U/mL penicillin (Life Technologies), and 100 mg/mL streptomycin (Life Technologies). HUDEP-2 cells, a gift from Y. Nakamura, were cultured as previously described (Vinjamur 2018). Briefly, HUDEP-2 cells were maintained in StemSpan SFEM (STEMCELL Technologies, catalog #09650) supplemented with stem cell factor (100 ng/mL; Miltenyi, catalog #130-096-696), dexamethasone (1 μM; Sigma-Aldrich, #D2915), doxycycline (2 μg/mL; Tocris Bioscience, catalog #4090), Erythropoietin (3 U/mL; STEMCELL Technologies), penicillin-streptomycin (100 U/mL; Gibco, catalog #15140-122), and GlutaMAX™ (100 U/mL; Gibco, catalog #35050061). Cells were passaged every 48 hours to maintain their density at 250,000-800,000 cells/mL. All cell lines were cultured in a humidified 5% CO_2 atmosphere at 37°C.

3.5 Generation of cellular models

3.5.1 Production of Lentiviral particles and infection of cell lines

Two different GIPZ lentiviral shRNA constructs targeting CDIN1 (V2LHS_159044) and SEC23B (V3LHS_3579749) were designed according to the manufacturer's instructions (https://horizondiscovery.com/en/genemodulation/knockdown/shrna/products/gipz-lentiviral-shrna). A non-silencing pGIPZ lentiviral shRNAmir was prepared as a control. Plasmids were digested with KpnI (Cat #FD0524), XhoI (Cat #FD0694), and NotI (Cat #ERO205) FastDigest Restriction Enzymes (Thermo Scientific). LentiX 293T cells were transfected with 9 µg/well of *CDIN1*-shRNA, *SEC23B*-shRNA, or CTR-shRNA plasmid, 30 µl of Trans-Lentiviral Packaging Mix (Horizon Inspired Cell Solutions), and 27 µl of FuGene HD Transfection Reagent (Promega). After 48 hours, cells were examined for TurboGFP expression. Supernatants containing pseudotyped lentiviral particles were harvested, centrifuged at 800 rpm for 10 min to remove cell debris filtered through a 0.45-µm, and stored at -80°C. Lentiviral particles (50 MOI) of sh-CTR, sh-CDIN1, and sh-SEC23B were used to infect HUDEP-2 cells (1.5 x 10^6), supplemented with 0.006 µg/µL Polybrene (TR-1003-G, Sigma). Similarly, sh-CTR and sh-SEC23B lentiviral particles were used to infect Hep3B-WT and Hep3B-PIEZO1-KI cells. After 48 hours, cells were maintained in puromycin (0.5 mg/mL for HUDEP-2 and 1.5 mg/mL for Hep3B) for 2 weeks and then sorted by FACS (FacsAria III, BD Biosciences) in collaboration with the Flow Cytometry Laboratory of CEINGE-Biotecnologie Avanzate. Sorted GFP^+ cells were assayed for *CDIN1* or *SEC23B* expression to verify clone stability.

3.5.2 Generation of HUDEP-2 PIEZO1-KI cells

Gain-of-function *PIEZO1* HUDEP-2 cells were generated through the introduction of the heterozygous *PIEZO1* variant R2456H using CRISPR/Cas9 technology. The specific mutation (c.7367G>A, p.R2456H) was confirmed by

PCR amplification of the targeted *PIEZO1* exon, followed by direct Sanger sequencing. The efficiency and specificity of the editing were further validated using ICE (Inference of CRISPR Edits) analysis.

3.6 Erythroid differentiation

To induce erythroid differentiation, HUDEP-2 cells were switched to differentiation media. The base differentiation media consists of Iscove's modified Dulbecco's medium (Sigma, catalog # FG0465) supplemented with GlutaMAX™ (100 U/mL; Gibco, catalog #35050061), penicillin-streptomycin (100 U/mL; Gibco, catalog #15140-122), human holo-transferrin (165ug/mL µg/ml; Sigma-Aldrich T4132), heparin (1 IU/mL; Sigma-Aldrich #H3149), recombinant human insulin (5 ug/mL; Sigma-Aldrich #91077C), 2.5% Human Serum Albumin (Sigma-Aldrich #A9731), Epogen (3 U/ml), doxycycline (1 µg/ml), and human stem cell factor (100 ng/mL; Miltenyi, catalog #130-096-696). The supplementation of hSCF and doxycycline to the differentiation media was stopped at days 4 and 7, respectively.

3.7 RNA isolation, reverse transcription, and quantitative real-time PCR analysis

Total RNA was extracted from cells using Trizol reagent (Life Technologies). Synthesis of cDNA from total RNA (1 µg) was performed using SensiFAST^{TM} cDNA Synthesis Kit (Bioline). Quantitative RT-PCR (qRT-PCR) was performed using the SYBR-green method, following standard protocols (ABI Prism 7900HT sequence detection system; Applied Biosystems). Real-time -PCR was performed using a standard TaqMan PCR kit protocol for *HBA*, *HBB*, *HBG*, *ID1,* and *ID3* genes. Relative gene expression was calculated by using the $2^{-\Delta Ct}$ method, as described (Russo 2013). The reactions were incubated in a 96-well plate at 95°C for 10 min, followed by 40 cycles of 95°C for 15 s and 60°C for 1 min.

3.8 Protein isolation and western blotting analysis

Proteins were extracted from cells using RIPA lysis buffer containing a protease inhibitor cocktail (Roche, Rotkreuz, Switzerland). Total protein extracts were analyzed by SDS-PAGE, and transferred to polyvinylidene difluoride membranes (BioRad, Milan, Italy), and then incubated with the required combinations of the following antibodies: rabbit anti-SEC23B (1:1000; SAB2102104; Sigma Aldrich); polyclonal rabbit anti- SEC23A (GTX109488 1:1000; GeneTex); rabbit anti-GAPDH (1:1000; 2118, Cell Signaling Technology); Rabbit anti-Ferritin (1:1000; abcam, ab75973); monoclonal rabbit anti-hemoglobin subunit alpha (1:1000, Abcam, ab92492); monoclonal rabbit anti-hemoglobin subunit beta (1:1000, Abcam, ab214049); monoclonal rabbit anti-fetal hemoglobin (1:1000, abcam, ab137096); monoclonal mouse anti-EpoR (1:1000, Invitrogen MA5-23824); monoclonal rabbit anti-Band3 (1:500, abcam, ab78067). The membranes were incubated with the enhanced chemiluminescence substrate (Supersignal West Pico chemiluminescent substrate kits; Thermo Fisher Scientific, Milan, Italy). Labeled bands were visualized, and densitometric analyses were performed with the BioRad Chemidoc using Quantity One software (BioRad) to obtain an integrated optical density (OD) value.

3.9 Flow Cytometry and Analysis

For each staining, 5×10^5 cells were collected from the culture at specific time points (days 0, 2, 4, 7, and 10) during the differentiation process. An unstained sample was included as a control for each set of measurements. HUDEP-2 cells were washed twice with phosphate-buffered saline (PBS) (Sigma-Aldrich, Munich, Germany) to remove residual medium and then incubated with a 100 µL staining mix. The mix contained the following fluorochrome-conjugated antibodies: APC-Vio770 anti-human CD235a (GPA) (1:200), VioGreen anti-human CD71 (1:100), PE-Vio770 anti-human CD36 (1:100), APC anti-human CD49d (1:200), PE anti-human Annexin V (1:100),

PerCP-Cy5.5 anti-human 7-AAD (1:100), and HV450 anti-human Hoechst 33342 (1:100), all purchased from Miltenyi Biotec. The cells were stained for 15 minutes at 4 °C in the dark to ensure optimal antibody binding. After staining, the cells were washed once with PBS to remove unbound antibodies and resuspended in 500 µL of PBS for flow cytometric analysis. A minimum of 0.5 × 10^5 cellular events per sample were recorded using a FACS flow cytometer (BD FACSDiva™). Data were analyzed and visualized using FlowJo_v10.9.0 software. Cells were first selected based on viability using 7-AAD staining. Erythroid sub-populations were categorized into three distinct groups, early, intermediate, and late, based on the inverse expression profiles of CD36 and GPA. Early erythroblasts were defined as $CD36^+/GPA^-$, intermediate as $CD36^+/GPA^+$, and late as $CD36^-/GPA^+$. This gating strategy was applied uniformly across all time points and models. Additionally, the percentage of enucleated erythroid cells was quantified using Hoechst staining, with enucleated populations identified as $Hoechst^-/GPA^+$.

3.10 RNA sequencing

RNA sequencing (RNA-seq) was performed on HUDEP-2 WT, HUDEP-2-PIEZO1-KI, HUDEP-2 sh-CTR, HUDEP-2 sh-CDIN1, and HUDEP-2 sh-SEC23B cells during erythroid differentiation. Briefly, mRNA libraries were prepared using the SureSelect XT HS2 mRNA Library Preparation System Protocol (Agilent Technologies) following the manufacturer's instructions. For samples with an RNA Integrity Number (RIN) >8, 1000 ng of total RNA was used. RNA quality and concentration were assessed using the RNA ScreenTape assay on a 4200 TapeStation (Agilent Technologies).

3.11 RNA-sequencing data analyses

Differential expression analysis of RNA-seq data was conducted using FPKM (Fragments per Kilobase of transcript per Million mapped reads) values calculated with Cufflinks software. For each comparison, data from three biological replicates were analyzed, with $\log_2(FC) \geq \pm 1.5$ and $-\log_{10}(\text{p-value}) \geq$

1.3 considered statistically significant. Differentially expressed genes were further analyzed to identify commonly deregulated pathways using KEGG (Kyoto Encyclopedia of Genes and Genomes) and Biological Processes (BP) annotations via the DAVID Bioinformatics Database (https://david.ncifcrf.gov/tools.jsp). Venn diagrams were generated using the Venny tool (https://bioinfogp.cnb.csic.es/tools/venny/) to identify shared or unique deregulated genes across conditions. Heatmaps were generated to visualize the temporal dynamics of gene expression across differentiation time points. For each gene, the fold change (FC) in expression was calculated at each differentiation day relative to the preceding day (Day 2 *vs* Day 0, Day 4 *vs* Day 2, Day 7 *vs* Day 4, and Day 10 *vs* Day 7). Visualization was performed using the pheatmap package in R, with Z-score normalization applied to rows. Rows were hierarchically clustered using Euclidean distance. Deconvolution analysis was based on RNA-seq data from HUDEP-2 sh-CTR, sh-CDIN1, and sh-SEC23B cells at five time points (days 0, 2, 4, 7, and 10). Computational deconvolution was conducted using CIBERSORTx software, which decomposes bulk RNA-seq data into distinct cellular components. A curated reference dataset representing transcriptional signatures of erythroid maturation stages, derived Hu (2013), was used as a reference to define five progenitor populations: proerythroblasts (ProE), early basophilic erythroblasts (EarlyBaso), late basophilic erythroblasts (LateBaso), polychromatic erythroblasts (Poly), and orthochromatic erythroblasts (Ortho).

3.12 Statistical analyses

Quantitative data were compared using the Mann-Whitney test for expression analysis between patients and controls. Differences in protein and gene expression levels between experimental groups were assessed using Student's t-test for pairwise comparisons. For multiple group comparisons, statistical significance was evaluated using two-way ANOVA, followed by

Tukey's multiple comparison test as a post-hoc analysis to adjust for multiple testing. A two-sided p-value < 0.05 was considered statistically significant.

7. Acknowledgments

I would like to express my profound gratitude to my tutor, Prof. Roberta Russo, for her support, guidance, and encouragement throughout my PhD journey. Her expertise, insightful advice, and constant availability have been important to both my professional and personal growth.

A special thanks goes to Prof. Immacolata Andolfo for her continuous motivation, and invaluable contributions, which have been a source of inspiration and assistance throughout my research.

Finally, I wish to thank Prof. Achille Iolascon for granting me the opportunity to conduct my research in his laboratory. His extraordinary example as a distinguished scientist has been a constant source of inspiration and has greatly enriched my academic journey.

8. List of publications

1. Rosato BE, Marra R, Del Giudice F, **Nostroso A**, Gobbi S, Bruschi B, Coccia P, Monaco V, Monti M, Iolascon A, Andolfo I, Russo R. One gene, two opposite phenotypes: a case report of hereditary anemia due to a loss-of-function variant in the EPAS1 gene. Haematologica. 2023 Oct 1;108(10):2872-2876.

2. Marra R, **Nostroso A**, Rosato BE, Esposito FM, D'Onofrio V, Iscaro A, Gambale A, Bruschi B, Coccia P, Poloni A, Unal S, Romano A, Iolascon A, Andolfo I, Russo R. Unveiling the genetic landscape of suspected congenital dyserythropoietic anemia type I: A retrospective cohort study of 36 patients. Am J Hematol. 2024 Aug;99(8):1511-1522.

3. Esposito FM, D'Onofrio V, Rosato BE, Marra R, **Nostroso A**, Iscaro A, Manno M, Ribersani M, Giorgi V, Celia R, Piscopo C, Iolascon A, Russo R, Andolfo I. Relevance of the E756del common variant in the PIEZO1 gene for haemolytic anaemia and hepatic iron overload. Br J Haematol. 2024 Nov 6.

4. Rosato BE, D'Onofrio V, Marra R, **Nostroso A**, Esposito FM, Iscaro A, Lasorsa VA, Capasso M, Iolascon A, Russo R, Andolfo I. RAS signaling pathway is essential in regulating PIEZO1-mediated hepatic iron overload in dehydrated hereditary stomatocytosis. Am J Hematol. 2024 Nov 18.

In preparation:

1. **Nostroso A**, Rosato BE, Marra R, Esposito FM, D'Onofrio V, Iscaro A, Ribersani M, Bulla A, Del Vecchio GC, Mandrile G, Ceglie T, Perrotta S, Iolascon A, Andolfo I, Russo R. Effect of multiple genetic variants in *SEC23B-PIEZO1* on iron metabolism dyshomeostasis in Hereditary anemias.

9. References

Ahmed MS, Shahjaman M, Kabir E, Kamruzzaman M. Structure modeling to function prediction of Uncharacterized Human Protein C15orf41. Bioinformation. 2018 May 31;14(5):206-212.

Andolfo I, Alper SL, De Franceschi L, Auriemma C, Russo R, De Falco L, Vallefuoco F, Esposito MR, Vandorpe DH, Shmukler BE, Narayan R, Montanaro D, D'Armiento M, Vetro A, Limongelli I, Zuffardi O, Glader BE, Schrier SL, Brugnara C, Stewart GW, Delaunay J, Iolascon A. Multiple clinical forms of dehydrated hereditary stomatocytosis arise from mutations in PIEZO1. Blood. 2013 May 9;121(19):3925-35, S1-12.

Andolfo I, Russo R, Gambale A, Iolascon A. Hereditary stomatocytosis: An underdiagnosed condition. Am J Hematol. 2018 Jan;93(1):107-121.

Andolfo I, Manna F, De Rosa G, Rosato BE, Gambale A, Tomaiuolo G, Carciati A, Marra R, De Franceschi L, Iolascon A, Russo R. PIEZO1-R1864H rare variant accounts for a genetic phenotype-modifier role in dehydrated hereditary stomatocytosis. Haematologica. 2018 Mar;103(3):e94-e97.

Andolfo I, Manna F, De Rosa G, Rosato BE, Gambale A, Tomaiuolo G, Carciati A, Marra R, De Franceschi L, Iolascon A, Russo R. PIEZO1-R1864H rare variant accounts for a genetic phenotype-modifier role in dehydrated hereditary stomatocytosis. Haematologica. 2018 Mar;103(3):e94-e97.

Andolfo I, Martone S, Rosato BE, Marra R, Gambale A, Forni GL, Pinto V, Göransson M, Papadopoulou V, Gavillet M, Elalfy M, Panarelli A, Tomaiuolo G, Iolascon A, Russo R. Complex Modes of Inheritance in Hereditary Red Blood Cell Disorders: A Case Series Study of 155 Patients. Genes (Basel). 2021 Jun 23;12(7):958.

Andolfo I, Rosato BE, Manna F, De Rosa G, Marra R, Gambale A, Girelli D, Russo R, Iolascon A. Gain-of-function mutations in PIEZO1 directly impair hepatic iron metabolism via the inhibition of the BMP/SMADs pathway. Am J Hematol. 2020 Feb;95(2):188-197.

Andolfo I, Rosato BE, Marra R, De Rosa G, Manna F, Gambale A, Iolascon A, Russo R. The BMP-SMAD pathway mediates the impaired hepatic iron metabolism associated with the ERFE-A260S variant. Am J Hematol. 2019 Nov;94(11):1227-1235.

Andolfo I, Russo R, Gambale A, Iolascon A. New insights on hereditary erythrocyte membrane defects. Haematologica. 2016 Nov;101(11):1284-1294.

Andolfo I, Russo R, Rosato BE, Manna F, Gambale A, Brugnara C, Iolascon A. Genotype-phenotype correlation and risk stratification in a cohort of 123 hereditary stomatocytosis patients. Am J Hematol. 2018 Dec;93(12):1509-1517.

Ask K, Jasencakova Z, Menard P, Feng Y, Almouzni G, Groth A. Codanin-1, mutated in the anaemic disease CDAI, regulates Asf1 function in S-phase histone supply. EMBO J. 2012 Apr 18;31(8):2013-23. doi: 10.1038/emboj.2012.55. Epub 2012 Mar 9. Erratum in: EMBO J. 2012 Jul 18;31(14):3229.

Ayas M, al-Jefri A, Baothman A, al-Mahr M, Mustafa MM, Khalil S, Karaoui M, Solh H. Transfusion-dependent congenital dyserythropoietic anemia type I successfully treated with allogeneic stem cell transplantation. Bone Marrow Transplant. 2002 Apr;29(8):681-2.

Babbs C, Roberts NA, Sanchez-Pulido L, McGowan SJ, Ahmed MR, Brown JM, Sabry MA; WGS500 Consortium; Bentley DR, McVean GA, Donnelly P, Gileadi O, Ponting CP, Higgs DR, Buckle VJ. Homozygous mutations in a predicted endonuclease are a novel cause of congenital dyserythropoietic anemia type I. Haematologica. 2013 Sep;98(9):1383-7.

Badens C, Guizouarn H. Advances in understanding the pathogenesis of the red cell volume disorders. Br J Haematol. 2016 Sep;174(5):674-85.

Camaschella C, Nai A. Ineffective erythropoiesis and regulation of iron status in iron loading anaemias. Br J Haematol. 2016 Feb;172(4):512-23.

Cappellini MD, Porter J, Origa R, Forni GL, Voskaridou E, Galactéros F, Taher AT, Arlet JB, Ribeil JA, Garbowski M, Graziadei G, Brouzes C, Semeraro M, Laadem A, Miteva D, Zou J, Sung V, Zinger T, Attie KM, Hermine O. Sotatercept, a novel transforming growth factor β ligand trap, improves anemia in β-thalassemia: a phase II, open-label, dose-finding study. Haematologica. 2019 Mar;104(3):477-484.

Casanovas G, Vujić Spasic M, Casu C, Rivella S, Strelau J, Unsicker K, Muckenthaler MU. The murine growth differentiation factor 15 is not essential for systemic iron homeostasis in phlebotomized mice. Haematologica. 2013 Mar;98(3):444-7.

Caulier A, Jankovsky N, Demont Y, Ouled-Haddou H, Demagny J, Guitton C, Merlusca L, Lebon D, Vong P, Aubry A, Lahary A, Rose C, Gréaume S, Cardon E, Platon J, Ouadid-Ahidouch H, Rochette J, Marolleau JP, Picard V, Garçon L. PIEZO1 activation delays erythroid differentiation of normal and hereditary xerocytosis-derived human progenitor cells. Haematologica. 2020 Mar;105(3):610-622.

Caulier AL, Sankaran VG. Molecular and cellular mechanisms that regulate human erythropoiesis. Blood. 2022 Apr 21;139(16):2450-2459.

Chasis JA, Mohandas N. Erythroblastic islands: niches for erythropoiesis. Blood. 2008 Aug 1;112(3):470-8.

Coste B, Xiao B, Santos JS, Syeda R, Grandl J, Spencer KS, Kim SE, Schmidt M, Mathur J, Dubin AE, Montal M, Patapoutian A. Piezo proteins are pore-forming subunits of mechanically activated channels. Nature. 2012 Feb 19;483(7388):176-81.

Crookston, J.H. , Godwin, T.F. , Wightman, K.J.R. , Dacie, J.V. , Davis, J.A. , Lewis, S.M. & Patterson, M.J.L. (1966) Congenital Dyserythropoietic Anaemia. Abstracts from XIth Congress of the International Society of Haematology, Sydney, pp. 18.

Da Costa L, Galimand J, Fenneteau O, Mohandas N. Hereditary spherocytosis, elliptocytosis, and other red cell membrane disorders. Blood Rev. 2013 Jul;27(4):167-78.

De Franceschi L, Turrini F, del Giudice EM, Perrotta S, Olivieri O, Corrocher R, Mannu F, Iolascon A. Decreased band 3 anion transport activity and band 3 clusterization in congenital dyserythropoietic anemia type II. Exp Hematol. 1998 Aug;26(9):869-73.

De Rosa G, Andolfo I, Marra R, Manna F, Rosato BE, Iolascon A, Russo R. RAP-011 Rescues the Disease Phenotype in a Cellular Model of Congenital Dyserythropoietic Anemia Type II by Inhibiting the SMAD2-3 Pathway. Int J Mol Sci. 2020 Aug 4;21(15):5577.

Dgany O, Avidan N, Delaunay J, Krasnov T, Shalmon L, Shalev H, Eidelitz-Markus T, Kapelushnik J, Cattan D, Pariente A, Tulliez M, Crétien A, Schischmanoff PO, Iolascon A, Fibach E, Koren A, Rössler J, Le Merrer M, Yaniv I, Zaizov R, Ben-Asher E, Olender T, Lancet D, Beckmann JS, Tamary H. Congenital dyserythropoietic anemia type I is caused by mutations in codanin-1. Am J Hum Genet. 2002 Dec;71(6):1467-74.

Ferreira R, Ohneda K, Yamamoto M, Philipsen S. GATA1 function, a paradigm for transcription factors in hematopoiesis. Mol Cell Biol. 2005 Feb;25(4):1215-27.

Gambale A, Iolascon A, Andolfo I, Russo R. Diagnosis and management of congenital dyserythropoietic anemias. Expert Rev Hematol. 2016 Mar;9(3):283-96.

Ganz T, Jung G, Naeim A, Ginzburg Y, Pakbaz Z, Walter PB, Kautz L, Nemeth E. Immunoassay for human serum erythroferrone. Blood. 2017 Sep 7;130(10):1243-1246.

Girelli D, Busti F, Brissot P, Cabantchik I, Muckenthaler MU, Porto G. Hemochromatosis classification: update and recommendations by the BIOIRON Society. Blood. 2022 May 19;139(20):3018-3029.

Gnanasambandam R, Bae C, Gottlieb PA, Sachs F. Ionic Selectivity and Permeation Properties of Human PIEZO1 Channels. PLoS One. 2015 May 8;10(5):e0125503.

Grootenboer S, Schischmanoff PO, Laurendeau I, Cynober T, Tchernia G, Dommergues JP, Dhermy D, Bost M, Varet B, Snyder M, Ballas SK, Ducot B, Babron MC, Stewart GW, Gasparini P, Iolascon A, Delaunay J. Pleiotropic syndrome of dehydrated hereditary stomatocytosis, pseudohyperkalemia, and perinatal edema maps to 16q23-q24. Blood. 2000 Oct 1;96(7):2599-605.

Gutiérrez L, Caballero N, Fernández-Calleja L, Karkoulia E, Strouboulis J. Regulation of GATA1 levels in erythropoiesis. IUBMB Life. 2020 Jan;72(1):89-105.

Han H, Rim YA, Ju JH. Recent updates of stem cell-based erythropoiesis. Hum Cell. 2023 May;36(3):894-907.

Heimpel H, Matuschek A, Ahmed M, Bader-Meunier B, Colita A, Delaunay J, Garcon L, Gilsanz F, Goede J, Högel J, Kohne E, Leichtle R, Munoz J, Perrotta S, Piscopo C, Renella R, Schwarz K, Smolenska-Sym G, Wickramasinghe S, Zanella A, Iolascon A. Frequency of congenital dyserythropoietic anemias in Europe. Eur J Haematol. 2010 Jul;85(1):20-5.

Hu J, Liu J, Xue F, Halverson G, Reid M, Guo A, Chen L, Raza A, Galili N, Jaffray J, Lane J, Chasis JA, Taylor N, Mohandas N, An X. Isolation and functional characterization of human erythroblasts at distinct stages: implications for understanding of normal and disordered erythropoiesis in vivo. Blood. 2013 Apr 18;121(16):3246-53.

Iolascon A, Andolfo I, Barcellini W, Corcione F, Garçon L, De Franceschi L, Pignata C, Graziadei G, Pospisilova D, Rees DC, de Montalembert M, Rivella S, Gambale A, Russo R, Ribeiro L, Vives-Corrons J, Martinez PA, Kattamis A, Gulbis B, Cappellini MD, Roberts I, Tamary H; Working Study Group on Red Cells and Iron of the EHA. Recommendations regarding splenectomy in hereditary hemolytic anemias. Haematologica. 2017 Aug;102(8):1304-1313.

Iolascon A, Esposito MR, Russo R. Clinical aspects and pathogenesis of congenital dyserythropoietic anemias: from morphology to molecular approach. Haematologica. 2012 Dec;97(12):1786-94.

Iolascon A, Heimpel H, Wahlin A, Tamary H. Congenital dyserythropoietic anemias: molecular insights and diagnostic approach. Blood. 2013 Sep 26;122(13):2162-6.

Iolascon A, Russo R, Esposito MR, Piscopo C, Asci R, De Falco L, Di Noce F. Congenital dyserythropoietic anaemias: new acquisitions. Blood Transfus. 2011 Jul;9(3):278-80.

Iolascon A, Andolfo I, Russo R. Congenital dyserythropoietic anemias. Blood. 2020 Sep 10;136(11):1274-1283.

Ishihara N, Hamasaki M, Yokota S, Suzuki K, Kamada Y, Kihara A, Yoshimori T, Noda T, Ohsumi Y. Autophagosome requires specific early Sec proteins for its formation and NSF/SNARE for vacuolar fusion. Mol Biol Cell. 2001 Nov;12(11):3690-702.

Johnstone RM. The Jeanne Manery-Fisher Memorial Lecture 1991. Maturation of reticulocytes: formation of exosomes as a mechanism for shedding membrane proteins. Biochem Cell Biol. 1992 Mar-Apr;70(3-4):179-90.

Kautz L, Jung G, Du X, Gabayan V, Chapman J, Nasoff M, Nemeth E, Ganz T. Erythroferrone contributes to hepcidin suppression and iron overload in a mouse model of β-thalassemia. Blood. 2015 Oct 22;126(17):2031-7.

Kautz L, Jung G, Valore EV, Rivella S, Nemeth E, Ganz T. Identification of erythroferrone as an erythroid regulator of iron metabolism. Nat Genet. 2014 Jul;46(7):678-84.

Kato K, Sugitani M, Kawataki M, Ohyama M, Aida N, Koga N, Ijiri R, Imaizumi K, Kigasawa H, Tanaka Y, Itani Y. Congenital dyserythropoietic anemia type 1 with fetal onset of severe anemia. J Pediatr Hematol Oncol. 2001 Jan;23(1):63-6.

Khoriaty R, Everett L, Chase J, Zhu G, Hoenerhoff M, McKnight B, Vasievich MP, Zhang B, Tomberg K, Williams J, Maillard I, Ginsburg D. Pancreatic SEC23B deficiency is sufficient to explain the perinatal lethality of germline SEC23B deficiency in mice. Sci Rep. 2016 Jun 14;6:27802.

Kim SE, Coste B, Chadha A, Cook B, Patapoutian A. The role of Drosophila Piezo in mechanical nociception. Nature. 2012 Feb 19;483(7388):209-12.

King R, Lin Z, Balbin-Cuesta G, Myers G, Friedman A, Zhu G, McGee B, Saunders TL, Kurita R, Nakamura Y, Engel JD, Reddy P, Khoriaty R. SEC23A rescues SEC23B-deficient congenital dyserythropoietic anemia type II. Sci Adv. 2021 Nov 26;7(48):eabj5293.

Kung C, Hixon J, Kosinski PA, Cianchetta G, Histen G, Chen Y, Hill C, Gross S, Si Y, Johnson K, DeLaBarre B, Luo Z, Gu Z, Yao G, Tang H, Fang C, Xu Y, Lv X, Biller S, Su SM, Yang H, Popovici-Muller J, Salituro F, Silverman L, Dang L. AG-348 enhances pyruvate kinase activity in red blood cells from patients with pyruvate kinase deficiency. Blood. 2017 Sep 14;130(11):1347-1356.

Lakhal S, Schödel J, Townsend AR, Pugh CW, Ratcliffe PJ, Mole DR. Regulation of type II transmembrane serine proteinase TMPRSS6 by hypoxia-inducible factors: new link between hypoxia signaling and iron homeostasis. J Biol Chem. 2011 Feb 11;286(6):4090-7.

Lakhal S, Schödel J, Townsend AR, Pugh CW, Ratcliffe PJ, Mole DR. Regulation of type II transmembrane serine proteinase TMPRSS6 by hypoxia-inducible factors: new link between hypoxia signaling and iron homeostasis. J Biol Chem. 2011 Feb 11;286(6):4090-7.

Lavabre-Bertrand T, Blanc P, Navarro R, Saghroun M, Vannereau H, Braun M, Wagner A, Taïb J, Lavabre-Bertrand C, Navarro M. alpha-Interferon therapy for congenital dyserythropoiesis type I. Br J Haematol. 1995 Apr;89(4):929-32.

Lin YC, Guo YR, Miyagi A, Levring J, MacKinnon R, Scheuring S. Force-induced conformational changes in PIEZO1. Nature. 2019 Sep;573(7773):230-234.

Lu Y, Hanada T, Fujiwara Y, Nwankwo JO, Wieschhaus AJ, Hartwig J, Huang S, Han J, Chishti AH. Gene disruption of dematin causes precipitous loss of erythrocyte membrane stability and severe hemolytic anemia. Blood. 2016 Jul 7;128(1):93-103.

Ma S, Dubin AE, Zhang Y, Mousavi SAR, Wang Y, Coombs AM, Loud M, Andolfo I, Patapoutian A. A role of PIEZO1 in iron metabolism in mice and humans. Cell. 2021 Feb 18;184(4):969-982.e13.

Marra R, Nostroso A, Rosato BE, Esposito FM, D'Onofrio V, Iscaro A, Gambale A, Bruschi B, Coccia P, Poloni A, Unal S, Romano A, Iolascon A, Andolfo I, Russo R. Unveiling the genetic landscape of suspected congenital dyserythropoietic anemia type I: A retrospective cohort study of 36 patients. Am J Hematol. 2024 Aug;99(8):1511-1522.

Merryweather-Clarke AT, Atzberger A, Soneji S, Gray N, Clark K, Waugh C, McGowan SJ, Taylor S, Nandi AK, Wood WG, Roberts DJ, Higgs DR, Buckle VJ, Robson KJ. Global gene expression analysis of human erythroid progenitors. Blood. 2011 Mar 31;117(13):e96-108.

Miano M, Eikema DJ, Aljurf M, Van't Veer PJ, Öztürk G, Wölfl M, Smiers F, Schulz A, Socié G, Vettenranta K, de Heredia CD, Zecca M, Maertens J, Rovira M, Sierra J, Uckan-Cetinkaya D, Skorobogatova E, Antmen AB, Dalle JH, Markiewicz M, Hamladji RM, Kitra-Roussou V, La Nasa G, Kriván G, Al-Seiraihy A, Giardino S, Risitano AM, de Latour RP, Dufour C. Stem cell transplantation for congenital dyserythropoietic anemia: an analysis from the European Society for Blood and Marrow Transplantation. Haematologica. 2019 Aug;104(8):e335-e339.

Muckenthaler MU, Rivella S, Hentze MW, Galy B. A Red Carpet for Iron Metabolism. Cell. 2017 Jan 26;168(3):344-361.

Murphy ZC, Getman MR, Myers JA, Burgos Villar KN, Leshen E, Kurita R, Nakamura Y, Steiner LA. Codanin-1 mutations engineered in human erythroid cells demonstrate role of CDAN1 in terminal erythroid maturation. Exp Hematol. 2020 Nov;91:32-38.e6.

Nair V, Das S, Sharma A. Hematopoietic stem cell transplantation in children with genetic defects. Indian Pediatr. 2009 Mar;46(3):241-3.

Narla A, Ebert BL. Ribosomopathies: human disorders of ribosome dysfunction. Blood. 2010 Apr 22;115(16):3196-205. doi: 10.1182/blood-2009-10-178129. Epub 2010 Mar 1.

Nemeth E, Tuttle MS, Powelson J, Vaughn MB, Donovan A, Ward DM, Ganz T, Kaplan J. Hepcidin regulates cellular iron efflux by binding to ferroportin and inducing its internalization. Science. 2004 Dec 17;306(5704):2090-3.

Noy-Lotan S, Dgany O, Lahmi R, Marcoux N, Krasnov T, Yissachar N, Ginsberg D, Motro B, Resnitzky P, Yaniv I, Kupfer GM, Tamary H. Codanin-1, the protein encoded by the gene mutated in congenital dyserythropoietic anemia type I (CDAN1), is cell cycle-regulated. Haematologica. 2009 May;94(5):629-37.

Olijnik AA, Roy NBA, Scott C, Marsh JA, Brown J, Lauschke K, Ask K, Roberts N, Downes DJ, Brolih S, Johnson E, Xella B, Proven M, Hipkiss R, Ryan K, Frisk P, Mäkk J, Stattin EM, Sadasivam N, McIlwaine L, Hill QA, Renella R, Hughes JR, Gibbons RJ, Groth A, McHugh PJ, Higgs DR, Buckle VJ, Babbs C. Genetic and functional insights into CDA-I prevalence and pathogenesis. J Med Genet. 2021 Mar;58(3):185-195.

Orvain C, Da Costa L, Van Wijk R, Pissard S, Picard V, Mansour-Hendili L, Cunat S, Giansily-Blaizot M, Cartron G, Schved JF, Aguilar-Martinez P. Inherited or acquired modifiers of iron status may dramatically affect the phenotype in dehydrated hereditary stomatocytosis. Eur J Haematol. 2018 Oct;101(4):566-569.

Orvain C, Da Costa L, Van Wijk R, Pissard S, Picard V, Mansour-Hendili L, Cunat S, Giansily-Blaizot M, Cartron G, Schved JF, Aguilar-Martinez P. Inherited or acquired modifiers of iron status may dramatically affect the phenotype in dehydrated hereditary stomatocytosis. Eur J Haematol. 2018 Oct;101(4):566-569.

Park SY, Matte A, Jung Y, Ryu J, Anand WB, Han EY, Liu M, Carbone C, Melisi D, Nagasawa T, Locascio JJ, Lin CP, Silberstein LE, De Franceschi L. Pathologic angiogenesis in the bone marrow of humanized sickle cell mice is reversed by blood transfusion. Blood. 2020 Jun 4;135(23):2071-2084.

Rapetti-Mauss R, Lacoste C, Picard V, Guitton C, Lombard E, Loosveld M, Nivaggioni V, Dasilva N, Salgado D, Desvignes JP, Béroud C, Viout P, Bernard M, Soriani O, Vinti H, Lacroze V, Feneant-Thibault M, Thuret I, Guizouarn H, Badens C. A mutation in the Gardos channel is associated with hereditary xerocytosis. Blood. 2015 Sep 10;126(11):1273-80.

Renella R, Roberts NA, Brown JM, De Gobbi M, Bird LE, Hassanali T, Sharpe JA, Sloane-Stanley J, Ferguson DJ, Cordell J, Buckle VJ, Higgs DR, Wood WG.

Codanin-1 mutations in congenital dyserythropoietic anemia type 1 affect HP1{alpha} localization in erythroblasts. Blood. 2011 Jun 23;117(25):6928-38.

Rosato BE, D'Onofrio V, Marra R, Nostroso A, Esposito FM, Iscaro A, Lasorsa VA, Capasso M, Iolascon A, Russo R, Andolfo I. RAS signaling pathway is essential in regulating PIEZO1-mediated hepatic iron overload in dehydrated hereditary stomatocytosis. Am J Hematol. 2024 Nov 18.

Rosato BE, Marra R, D'Onofrio V, Del Giudice F, Della Monica S, Iolascon A, Andolfo I, Russo R. SEC23B Loss-of-Function Suppresses Hepcidin Expression by Impairing Glycosylation Pathway in Human Hepatic Cells. Int J Mol Sci. 2022 Jan 24;23(3):1304.

Roy NBA, Babbs C. The pathogenesis, diagnosis and management of congenital dyserythropoietic anaemia type I. Br J Haematol. 2019 May;185(3):436-449.

Roy NBA, Babbs C. The pathogenesis, diagnosis and management of congenital dyserythropoietic anaemia type I. Br J Haematol. 2019 May;185(3):436-449.

Russo R, Andolfo I, Manna F, De Rosa G, De Falco L, Gambale A, Bruno M, Mattè A, Ricchi P, Girelli D, De Franceschi L, Iolascon A. Increased levels of ERFE-encoding *FAM132B* in patients with congenital dyserythropoietic anemia type II. Blood. 2016 Oct 6;128(14):1899-1902.

Russo R, Esposito MR, Iolascon A. Inherited hematological disorders due to defects in coat protein (COP)II complex. Am J Hematol. 2013 Feb;88(2):135-40.

Russo R, Iolascon A, Andolfo I, Marra R, Rosato BE. Updates on clinical and laboratory aspects of hereditary dyserythropoietic anemias. Int J Lab Hematol. 2024 Aug;46(4):595-605.

Russo R, Marra R, Andolfo I, De Rosa G, Rosato BE, Manna F, Gambale A, Raia M, Unal S, Barella S, Iolascon A. Characterization of Two Cases of Congenital Dyserythropoietic Anemia Type I Shed Light on the Uncharacterized C15orf41 Protein. Front Physiol. 2019 May 22;10:621.

Russo R, Marra R, Rosato BE, Iolascon A, Andolfo I. Genetics and Genomics Approaches for Diagnosis and Research Into Hereditary Anemias. Front Physiol. 2020 Dec 22;11:613559.

Schwarz K, Iolascon A, Verissimo F, Trede NS, Horsley W, Chen W, Paw BH, Hopfner KP, Holzmann K, Russo R, Esposito MR, Spano D, De Falco L, Heinrich K, Joggerst B, Rojewski MT, Perrotta S, Denecke J, Pannicke U, Delaunay J, Pepperkok R, Heimpel H. Mutations affecting the secretory COPII coat component SEC23B cause congenital dyserythropoietic anemia type II. Nat Genet. 2009 Aug;41(8):936-40.

Scott C, Downes DJ, Brown JM, Beagrie R, Olijnik AA, Gosden M, Schwessinger R, Fisher CA, Rose A, Ferguson DJP, Johnson E, Hill QA, Okoli

S, Renella R, Ryan K, Brand M, Hughes J, Roy NBA, Higgs DR, Babbs C, Buckle VJ. Recapitulation of erythropoiesis in congenital dyserythropoietic anaemia type I (CDA-I) identifies defects in differentiation and nucleolar abnormalities. Haematologica. 2021 Nov 1;106(11):2960-2970.

Sedor SF, Shao S. Mechanism of ASF1 Inhibition by CDAN1. bioRxiv [Preprint]. 2024 Aug 8:2024.08.08.607204.

Shih HM, Wu CJ, Lin SL. Physiology and pathophysiology of renal erythropoietin-producing cells. J Formos Med Assoc. 2018 Nov;117(11):955-963.

Shroff M, Knebel A, Toth R, Rouse J. A complex comprising C15ORF41 and Codanin-1: the products of two genes mutated in congenital dyserythropoietic anaemia type I (CDA-I). Biochem J. 2020 May 29;477(10):1893-1905.

Siatecka M, Bieker JJ. The multifunctional role of EKLF/KLF1 during erythropoiesis. Blood. 2011 Aug 25;118(8):2044-54.

Silvestri L. Ironing erythroid cells takes FLG1 and ERFE to tango. Blood. 2024 Mar 28;143(13):1208-1209

Su AI, Wiltshire T, Batalov S, Lapp H, Ching KA, Block D, Zhang J, Soden R, Hayakawa M, Kreiman G, Cooke MP, Walker JR, Hogenesch JB. A gene atlas of the mouse and human protein-encoding transcriptomes. Proc Natl Acad Sci U S A. 2004 Apr 20;101(16):6062-7.

Swickley G, Bloch Y, Malka L, Meiri A, Noy-Lotan S, Yanai A, Tamary H, Motro B. Characterization of the interactions between Codanin-1 and C15Orf41, two proteins implicated in congenital dyserythropoietic anemia type I disease. BMC Mol Cell Biol. 2020 Mar 23;21(1):18.

Syfuss PY, Ciupea A, Brahimi S, Cynober T, Stewart GW, Grandchamp B, Beaumont C, Tchernia G, Delaunay J, Wagner JC. Mild dehydrated hereditary stomatocytosis revealed by marked hepatosiderosis. Clin Lab Haematol. 2006 Aug;28(4):270-4.

Tamary H, Dgany O. Congenital Dyserythropoietic Anemia Type I. 2009 Apr 21 [updated 2021 Jul 29]. In: Adam MP, Feldman J, Mirzaa GM, Pagon RA, Wallace SE, Amemiya A, editors. GeneReviews® [Internet]. Seattle (WA): University of Washington, Seattle; 1993–2024.

Tamary H, Shalev H, Perez-Avraham G, Zoldan M, Levi I, Swinkels DW, Tanno T, Miller JL. Elevated growth differentiation factor 15 expression in patients with congenital dyserythropoietic anemia type I. Blood. 2008 Dec 15;112(13):5241-4.

Tanno T, Bhanu NV, Oneal PA, Goh SH, Staker P, Lee YT, Moroney JW, Reed CH, Luban NL, Wang RH, Eling TE, Childs R, Ganz T, Leitman SF, Fucharoen

S, Miller JL. High levels of GDF15 in thalassemia suppress expression of the iron regulatory protein hepcidin. Nat Med. 2007 Sep;13(9):1096-101.

Tao J, Zhu M, Wang H, Afelik S, Vasievich MP, Chen XW, Zhu G, Jensen J, Ginsburg D, Zhang B. SEC23B is required for the maintenance of murine professional secretory tissues. Proc Natl Acad Sci U S A. 2012 Jul 17;109(29):E2001-9.

Tóthová Z, Šemeláková M, Solárová Z, Tomc J, Debeljak N, Solár P. The Role of PI3K/AKT and MAPK Signaling Pathways in Erythropoietin Signalization. Int J Mol Sci. 2021 Jul 19;22(14):7682.

Vinjamur DS, Bauer DE. Growing and Genetically Manipulating Human Umbilical Cord Blood-Derived Erythroid Progenitor (HUDEP) Cell Lines. Methods Mol Biol. 2018;1698:275-284.

Wang CY, Xu Y, Traeger L, Dogan DY, Xiao X, Steinbicker AU, Babitt JL. Erythroferrone lowers hepcidin by sequestering BMP2/6 heterodimer from binding to the BMP type I receptor ALK3. Blood. 2020 Feb 6;135(6):453-456.

Xu G, van Bruggen R, Gualtieri CO, Moradin N, Fois A, Vallerand D, De Sa Tavares Russo M, Bassenden A, Lu W, Tam M, Lesage S, Girouard H, Avizonis DZ, Deblois G, Prchal JT, Stevenson M, Berghuis A, Muir T, Rabinowitz J, Vidal SM, Fodil N, Gros P. Bisphosphoglycerate Mutase Deficiency Protects against Cerebral Malaria and Severe Malaria-Induced Anemia. Cell Rep. 2020 Sep 22;32(12):108170.

Zaninoni A, Marra R, Fermo E, Consonni D, Andolfo I, Marcello AP, Rosato BE, Vercellati C, Barcellini W, Iolascon A, Bianchi P, Russo R. Evaluation of the main regulators of systemic iron homeostasis in pyruvate kinase deficiency. Sci Rep. 2023 Mar 16;13(1):4395.

Zarychanski R, Schulz VP, Houston BL, Maksimova Y, Houston DS, Smith B, Rinehart J, Gallagher PG. Mutations in the mechanotransduction protein PIEZO1 are associated with hereditary xerocytosis. Blood. 2012 Aug 30;120(9):1908-15.

Zarychanski R, Schulz VP, Houston BL, Maksimova Y, Houston DS, Smith B, Rinehart J, Gallagher PG. Mutations in the mechanotransduction protein PIEZO1 are associated with hereditary xerocytosis. Blood. 2012 Aug 30;120(9):1908-15.

Zhou D, Liu K, Sun CW, Pawlik KM, Townes TM. KLF1 regulates BCL11A expression and gamma- to beta-globin gene switching. Nat Genet. 2010 Sep;42(9):742-4.